https://doi.org/10.5194/egusphere-2025-4636
Preprint. Discussion started: 14 October 2025

MAESTRO instrument operation and performance over two decades in orbit

Jiansheng Zou[1], C. Thomas McElroy[2], James R. Drummond[1,3], Kaley A. Walker[1], Paul S. Jeffery[1]

1. Department of Physics, University of Toronto, Toronto, Ontario, M5S 1A7, Canada
2. Department of Earth and Space Science and Engineering, York University, Toronto, Ontario, M3J 1P3, Canada
3. Department of Physics and Atmospheric Physics, Dalhousie University, Halifax, Nova Scotia, B3H 4R2, Canada

Correspondence: Jiansheng Zou (jzou@atmosp.physics.utoronto.ca)

Abstract

MAESTRO (Measurement of Aerosol Extinction in the Stratosphere and Troposphere Retrieved by Occultation), a dual UV (ultraviolet) and Visible-NIR (visible-near-infrared) spectrometer, has been operating aboard the Canadian satellite SCISAT for over 21 years. Recently, MAESTRO version 4.5 data products were released, consisting of volume mixing ratio profile data for NO_2 and O_3 retrieved from the UV channel, as well as a separate O_3 product from the Visible-NIR channel. An aerosol extinction product is currently under development. Motivated by the instrument's longevity, this paper will review the MAESTRO operations and performance over its lifetime, examining the key issues that impact its retrievals of atmospheric constituents. These include: a) the design of the MAESTRO spectrometer measurement schemes for sunset and sunrise occultations, including the role of long-term changes in the measured spectral intensities from the UV and Visible-NIR spectrometers, b) the determination of the position of the MAESTRO field of view (FOV) on the Sun, c) changes in the MAESTRO FOV position during occultations, including the impacts of this on the Level 1 transmittance calculation(s), d) understanding the relative position between the MAESTRO FOV and the ACE-FTS (Atmospheric Chemistry Experiment – Fourier Transform Spectrometer) FOV which are crucial for incorporating the input ACE-FTS atmosphere data in the Level 2 retrieval, e) verifying on-orbit the wavelength assignment at the detector arrays affected by a sudden persistent change in the instrument's

https://doi.org/10.5194/egusphere-2025-4636
Preprint. Discussion started: 14 October 2025

thermal environment, and f) the approaches taken to determine the MAESTRO measurement tangent heights, which are the pivotal steps in the MAESTRO retrieval of atmospheric constituents.

1. Introduction

The MAESTRO instrument (Measurement of Aerosol Extinction in the Stratosphere and Troposphere Retrieved by Occultation; McElroy et al. 2007) is aboard the Canadian SCISAT satellite, alongside the ACE-FTS (Atmospheric Chemistry Experiment − Fourier Transform Spectrometer) instrument, as part of the ACE (Atmospheric Chemistry Experiment) mission (Bernath et al., 2005). MAESTRO utilizes the widely used solar occultation technique to make atmospheric absorption spectrum measurements. This technique enables the self-calibration of atmospheric absorption spectra, thereby rendering them insensitive to long-term drifts in the instrument's gain (McCormick et al., 1989). Due to the small field of view (FOV) in the elevation direction of these measurements on the limb, they also possess high vertical resolution. The latest MAESTRO measurement products have been compared against other instruments in Jeffery et al. (2025), who found good agreement.

Over the past four decades, there have been several solar occultation UV-Visible-NIR (ultraviolet-visible-near-infrared) spectrometers in orbit, including: SAGE I (1979−1981; McCormick et al., 1989), SAGE II (1984−2005; Damadeo et al., 2013), SAGE III/M3M (2001−2006; Wang et al., 2006), and SAGE III/ISS (2017−present; McCormick et al., 2020); however, MAESTRO was the sole solar occultation instrument in orbit between 2006 and 2017. Using these instruments, a merged continuous occultation record spanning four decades, from 1984 to the present, can be constructed.

The other ACE instrument, ACE-FTS, also uses the solar occultation technique to make measurements and is boresighted with MAESTRO using a common sun tracker. It also has two Imagers, one operating in the Visible and the other at NIR wavelengths, with respective nominal wavelengths of

https://doi.org/10.5194/egusphere-2025-4636
Preprint. Discussion started: 14 October 2025

525 nm and 1020 nm, which take sun images during solar occultations at a frequency of one image every 0.25 seconds (Gilbert et al., 2007). The most recent version of the ACE-FTS data, version 5.3 (Boone et al., 2023; accessible at https://databace.scisat.ca/level2/ace_v5.3/, registration required), contains volume mixing ratio (VMR) measurements of over 70 atmospheric molecules and isotopologues and aerosol extinction profiles from the ACE Visible and NIR channel Imagers.

MAESTRO measures approximately the same air mass as ACE-FTS but can measure at lower altitudes and with higher vertical resolution than ACE-FTS (McElroy et al., 2007). The main MAESTRO Level 1 and Level 2 data products include: v4.5 NO_2 and O_3 data (Jeffery et al., 2025; accessible at https://databace.scisat.ca/level2/mae_v4.5/), v3.13 aerosol extinction data (Khanal et al., 2024), v3.12.1 aerosol extinction data (Robert et al., 2016), and v2.2 and v3.12.1/2 optical depth data which have been used for independent water vapour retrievals (Sioris et al., 2010, 2016a, 2016b).

The primary focus of this study is to evaluate the in-flight performance of key elements of MAESTRO, to assess the issues that have arisen during operations, and to evaluate the impact of anomalous events on the instrument's health and ability to retrieve atmospheric constituents.

Following a brief overview of the instrument itself in Section 2, these elements are addressed in Section 3. Section 3.1 presents the operational schemes (termed "action tables") that define the MAESTRO measurement sequences, with specific attention paid to changes in the beta-angle (the angle between the satellite orbital plane and the Sun−Earth vector), the large dynamic range of integration times over the occultation period, the saturation of detector signals, the measurement tangent height range, and the vertical resolution of the instrument. Section 3.2 examines derived information about the UV and Visible-NIR slit positions, which is crucial to an understanding of the MAESTRO measurements, as these slits direct sunlight to the spectrometers and thereby determine the instrument's FOVs over the Sun via their projected positions on the Sun. The slit positions are examined using results

https://doi.org/10.5194/egusphere-2025-4636
Preprint. Discussion started: 14 October 2025

from in-flight sun-scan experiments and are compared with pre-flight test data. The relative positions of the MAESTRO's slits to the ACE-FTS FOV on the Sun are also assessed. Section 3.3 further explores the MAESTRO FOV with a case study of the change in the FOV location on the Sun during an occultation. The impact of temperature variations on the instrument's performance is examined in Sect. 3.4 and 3.5, focusing in the former on periodic variations in temperatures, and in the latter on the thermal impact of the satellite's star tracker failure on 17 June 2015. Within this, the potential of this anomaly to lead to anomalous behaviour in the rotation of the ACE Imagers and the MAESTRO slits is discussed, as well as the assigned wavelengths of the spectrometers. In Sect. 3.6, the stability of the spectrometer over the mission is presented, highlighting the trends of the high sun spectra.

MAESTRO's retrievals are not stand-alone but use ACE-FTS-derived atmospheric temperature and pressure information for each occultation for their reference atmosphere. Complicating the use of the ACE-FTS temperature and pressure fields for the MAESTRO retrievals, it was found early in the mission that the time recorded by MAESTRO was inconsistent with that recorded by ACE-FTS (McElroy et al., 2007). This time difference coupled with the issue of an uncertain relationship between the observation angles of the ACE-FTS and MAESTRO, poses a challenge for the MAESTRO retrievals. Section 3.7 discusses several approaches that have used ACE-FTS data as the reference atmosphere for MAESTRO retrievals.

2. The MAESTRO Instrument

A detailed description of the MAESTRO instrument, operational principles, subsystems, and the general retrieval method is given in McElroy et al. (2007). In brief, MAESTRO is composed of two spectrometers, one measuring in the UV (285−565 nm) and the other in the Visible-NIR (515−1015 nm). Each consists of a telescope, lens, slit, concave holographic grating, and a 1024-element photodiode

https://doi.org/10.5194/egusphere-2025-4636
Preprint. Discussion started: 14 October 2025

array detector, as schematically displayed in Fig. 1 (McElroy et al., 2007). MAESTRO shares a common sun tracker and optical bore with ACE-FTS. Incoming sunlight passes through the telescope-lens-slit path, is diffracted by the diffraction grating, and reaches the detectors.

MAESTRO's detectors are connected to a field-programmable gate array (FPGA) based microprocessor system with an autonomous FPGA controller and data readout peripheral that is pre-loaded with the modes and integration times for each individual spectral measurement. This readout system controls the detector timing, reads the data out through a 16-bit A/D converter, and handles the co-adding of spectra (McElroy et al., 2007). The detector readout boards communicate with the MAESTRO instrument control (MIC) computer through synchronous embedded state machines. During observations, the state machine turns off the microprocessor clock to prevent asynchronous noise. The action table measurement schemes, uploaded from the ground to the MIC via commands from the spacecraft bus, are critical to MAESTRO operation as they define measurement sequences for different scenarios (e.g., sunset, sunrise, high sun, etc.).

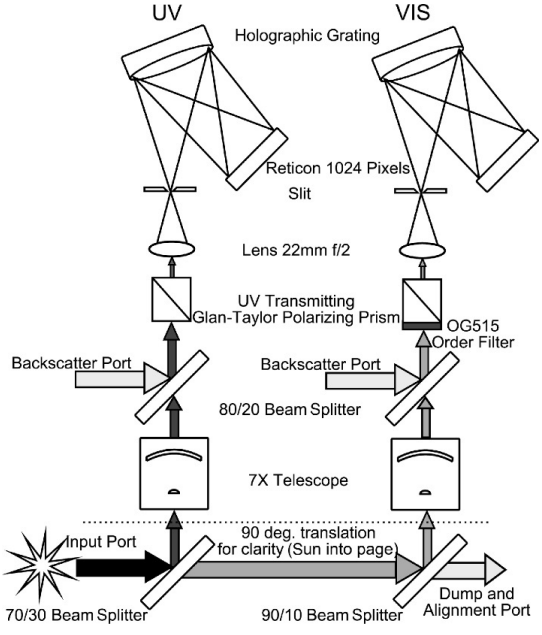

https://doi.org/10.5194/egusphere-2025-4636
Preprint. Discussion started: 14 October 2025

Figure 1 A schematic of the MAESTRO instrument with UV and Visible-NIR spectrometers (adapted from McElroy et al. (2007), Applied Optics, 46 (20), 4341-4356, licensed under CC BY-NC 4.0).

3. MAESTRO operations

3.1 Development of MAESTRO measurement schemes - action tables

The method by which the detectors capture signals through the extreme dynamic range over which MAESTRO observes is described in McElroy et al. (2007) and Nowlan et al. (2007). Crucially, two parameters, specified by action tables, control the detector readout throughout a measurement: the integration time (the exposure time of the detector to sunlight, referred to as a "tic", lasting 0.2 μs) and the group of pixels. A group comprises 2^n pixels (n=0−10) which are reset simultaneously. At the highest detector signals, each pixel is reset with a short integration time (1024 groups of 1 pixel) in sequence. At the lowest signal levels with a long integration time, the entire array of 1024 pixels is reset simultaneously (1 group of 1024 pixels). Between these two extremes for integration and measurement, by changing pixel groups and the integration time, the signal-to-noise ratio is optimized throughout the occultation. It takes about 330 ms to complete a full spectral measurement across the different groups (McElroy et al., 2007).

MAESTRO uses 19 different combinations of pixel groups and integration times during an occultation measurement, collecting 80 spectra spanning tangent heights between 0 and approximately 150 km for sunrise or the reverse for sunset. These provide atmospheric measurements (0–100 km) and exo-atmospheric measurements (100–150 km and above) for sunrise and sunset measurements. MAESTRO also collects 80 dark count spectra by taking measurements on the orbit dark side with the same occultation action tables for measuring a zero-irradiance point. Special action tables, such as sun-scans, have also been created for specific events and tests.

https://doi.org/10.5194/egusphere-2025-4636
Preprint. Discussion started: 14 October 2025

Action tables must account for changes in the observation beta angle, which ranges between 0° to 60°, and the corresponding variation in the atmospheric measurement period, which ranges from 63 seconds to about 190 seconds. Action tables at beta angle sub-ranges are generated from the table at zero beta angle by extending the time intervals between spectral measurements. The detector modes and integration times of each spectral measurement are fixed.

Between February 2004 and August 2005, five beta angle sub-ranges were used to define the MAESTRO action table set "A", with sub-range bounds at 0°, 20°, 30°, 45°, 55°, and 60 °. The timing of the five sunset and sunrise action tables is based on the centre of these beta angle sub-ranges.

Figure 2 shows an example of a spectral measurement time sequence for observation ss8342 (an observation is catalogued by sunset (ss) or sunrise (sr) and the orbit number) on 1 March 2005 using the "A" tables and at a beta angle of 38°. Here, 80 data points are plotted (with a guideline), corresponding to integrated spectrum intensities measured during a sunset occultation from the UV (Fig. 2a) and Visible-NIR (Fig. 2b) spectrometers. These 80 data points cover the altitude range from approximately 150 km to near 0 km. The altitude information is derived from the ACE-FTS tangent height data, which are time-tagged (see Sect. 3.7 for a discussion on time-tagging) and cover a range of ~10−120 km. The first 20 exo-atmospheric spectra are averaged as the high-sun reference. Between about 50 and 30 km, 8 spectra are recorded; between 30 and 15 km, 15; and below 15 km, 27. The integration time and the number of repetitions for each row of the action table are shown in the legends of Fig. 2a and 2b. Due to the geometric weighting of the absorption in the tangent layer relative to that of the layer above in the spherical atmosphere (McElroy et al., 2007), the vertical resolution of the retrieved profiles is about ~1 km, roughly matching the vertical sampling in the troposphere and stratosphere.

For measurement ss8342, the 80 spectra recorded using the 19 rows specified in the action table are shown in Figs. 2c and 2d for the UV and Visible-NIR channels, respectively. The integration time for

https://doi.org/10.5194/egusphere-2025-4636
Preprint. Discussion started: 14 October 2025

the UV channel varies from 740 tics at the high sun to 750365 tics at the near-zero tangent height, and for the Visible-NIR channel, it varies from 1540 tics at the high sun to 12425 tics at zero tangent height.

Early in the mission lifetime, it was discovered that some of the sunrise spectra measurements were invalid due to a delayed start of the measurement sequence, which caused the detector signal to saturate. This led to a redefinition of the measurement start time from a fixed time offset to a tangent height-derived time offset, starting on 9 February 2005.

Additionally, the set "A" of action tables was found to have an overly high density of data points recorded at low altitudes (below 15 km), as illustrated in Figure 2, and there are notable mismatches between the measurement time and the variable occultation time within each beta angle subrange. Therefore, a second set of action tables, "B," was developed with more data points at higher altitudes (above 15 km), fewer at lower altitudes (below 15 km), and with more beta angle ranges covering nine intervals with sub-range bounds at 0°, 10°, 25°, 34°, 42.5°, 48.5°, 53.2°, 56.7°, 58.2°, and 59.4°. Here, 79 atmospheric spectral measurements are taken between 0 and 100 km, with one at 150 km. For the exo-atmospheric spectrum, a separate scheme of 20 spectral high-sun measurements above 150 km was produced and included in the "B" tables.

Figure 3 shows an example of a spectral measurement time sequence for observation ss11053 on 1 September 2005 with a beta angle of 38° using the "B" tables. One upper limit occultation measurement is taken at 150 km, and the high-sun reference spectra were collected with a separate action table of 20 measurements above 150 km (not shown here). With this newer measurement table set "B", most measurement points are now located within the ozone layer. From 50 km to 25 km, there are 34 points; from 25 km to 20 km, 10; and from 20 km to 15 km, there are 7. On average, there are 1.5 measurements per 1 km. In Figs. 3a/b, spectral intensities at very low altitudes, well below the lowest ACE-FTS measurement altitude, are very small and cut off. Compared to table A (Figs. 2a/b) with a

https://doi.org/10.5194/egusphere-2025-4636
Preprint. Discussion started: 14 October 2025

similar beta angle, the occultation measurement time for table B (Figs. 3a/b) is longer by about 5 seconds, so the measurements using set "B" cover wider altitude ranges than using set "A". The set "B" action tables have been in use since 1 August 2005. For a nominal occultation, the action tables for high sun, occultation, and dark count observations together constitute a complete set for performing a retrieval.

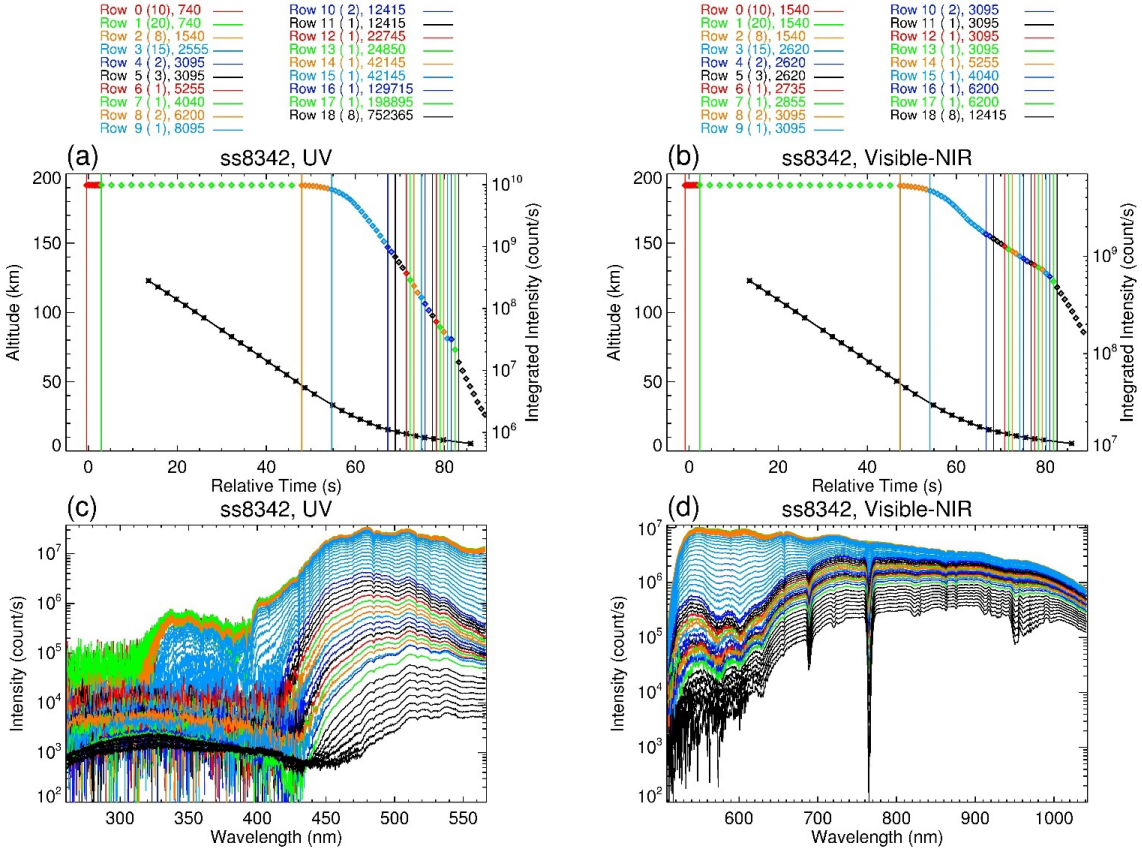

Figure 2 MAESTRO spectral measurement during a sunset occultation ss8342 on 1 March 2005 at 01:38:54z (30 km tangent height), located at 80.004° N, 161.137° W, and with a beta angle of 38.099° using an action table in set "A" applicable to the beta angle range of 30−45°. Panel a (top left) shows the integrated UV spectrum intensity vs. time with the colour code specified in the legend on the top of the

https://doi.org/10.5194/egusphere-2025-4636
Preprint. Discussion started: 14 October 2025

panel and the tangent height vs. time curve (black) obtained from the ACE-FTS data. The MAESTRO and ACE-FTS times are aligned as established in Sect. 3.7. The left y-axis indicates the altitude, and the right y-axis the integrated spectrum intensity. The coloured text lists the 19 rows of an action table in set "A", each marked by a colour code, with the number of repetitions for the row in parentheses and the integration time in tics. The vertical lines denote the start time of each row. Panel b (top right) is similar to (a) but for the Visible-NIR channel. Panel c (bottom left) shows the 80 UV spectra produced using the action table with the same colour code indicated in (a), and Panel d (bottom right) is similar to (c) but for the Visible-NIR.

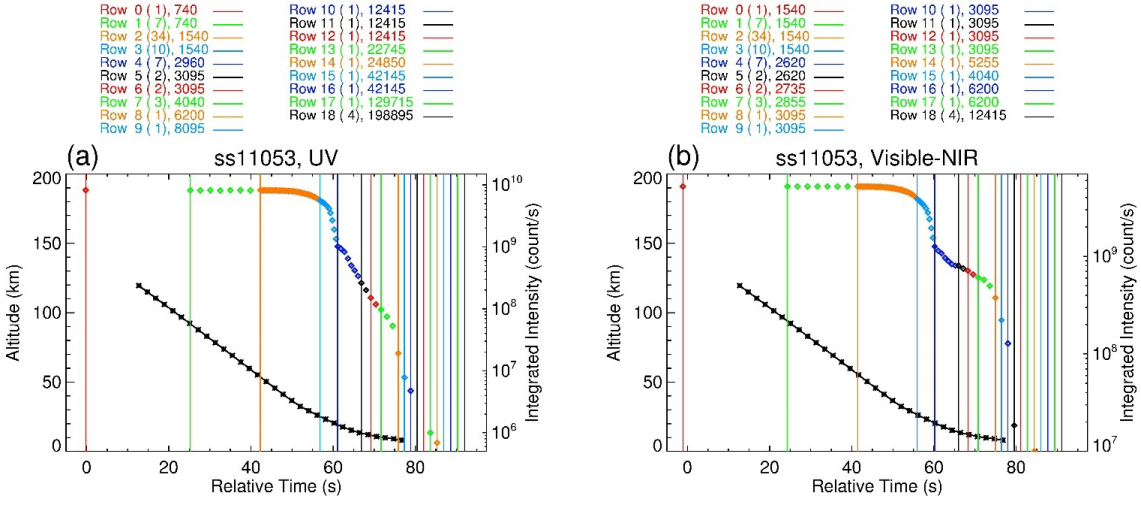

Figure 3: Like Fig. 2a and 2b but for measurement of occultation ss11053 on 1 September 2005 at 00:47:12z (30 km tangent height), 79.265° S, 152.432° W, and with a beta angle of -38.037° using an action table in set "B" applicable to the beta angle range of 34−42.5°.

3.2 MAESTRO slits projected on the ACE Imagers

The MAESTRO instrument views the Sun through two separate narrow slits: one for the UV spectrometer and the other for the Visible-NIR spectrometer (Fig. 1). The projection of the slits on the

https://doi.org/10.5194/egusphere-2025-4636
Preprint. Discussion started: 14 October 2025

Sun is nominally 0.022° (elevation) x 0.65° (azimuth) for the UV and 0.022° x 0.89° for the Visible-NIR channel (McElroy et al., 2007). The elevation projection is much smaller than the sun diameter, while the azimuth projection is larger, as the sun angular diameter is about 0.5°. Knowing the location of MAESTRO's slits relative to the Sun and to the ACE-FTS FOV is important because the former is needed for accurate Level 1 transmittance calculation and for understanding issues in the Level 1 data, especially for lower altitudes (see Sect. 3.3), while the latter is important for use of the ACE-FTS reference atmosphere (see Sect. 3.7). Ideally, the UV and Visible-NIR slits would a) be parallel to the Earth's horizon, ensuring that the lines of sight (LOS) through all points on the slit exhibit an almost homogeneous atmospheric distribution, b) fixed at the Sun's centre during the occultation to maintain a stable irradiance source from the Sun that is unaffected by the deformation of the solar disk at low altitudes, and c) overlap with the ACE-FTS FOV, allowing the ACE-FTS derived temperature and pressure profile data to be directly utilized as the MAESTRO reference atmosphere.

Pre-launch tests of the slit locations on the ACE Imagers were conducted at the Canadian Space Agency's David Florida Laboratory, Ottawa, Canada. Following the launch, a series of sun-scan observations were made to verify their locations. A sun-scan procedure includes elevation scans (upwards and downwards across the Sun) at zero, positive, and negative azimuth offsets, as well as a separate azimuth scan. The sun-scan measurements took place on 16-17 February 2004, 21 February 2004, 24-25 June 2004, 8 December 2004, and 15-17 December 2004. The relative positions of the MAESTRO slits and the ACE Imagers are fixed, so during these sun-scans, images of the Sun are acquired at 4 Hz, enabling the identification of the slit locations on the Sun.

During an elevation scan, as the slit traverses the Sun, the MAESTRO spectral intensities reach their maxima when the slit is centred on the Sun. The location of the maximum is determined for both the UV

https://doi.org/10.5194/egusphere-2025-4636
Preprint. Discussion started: 14 October 2025

and Visible-NIR data. Three sets of points are obtained from each of three azimuth offsets, and notionally, these points form a line aligned with the slit.

During an azimuth scan, the slit does not necessarily pass through the centre of the Sun. These scans begin off the Sun, and the intensity increases until the slit encompasses the Sun, indicated by an intensity plateau, before declining as the slit moves off from the Sun. The integrated MAESTRO half-intensity yields the locations of the edges of the slit in the azimuth direction.

Figure 4 illustrates the UV and Visible-NIR integrated intensities measured during a set of sun scans conducted on 8 December 2004, including an elevation scan (Fig. 4a), elevation scans with positive/negative azimuth offsets (Figs. 4b/c), and an azimuth scan (Fig. 4d). There are two peaks in intensity during each elevation scan procedure, one during the upward scan and the other during the downward scan. The positions of the Sun's centre are determined when the UV and Visible-NIR spectra reach their maxima in the elevation scans. For an azimuth scan, the times at the half maximum intensity are identified (Fig. 4d), allowing for the identification of the locations of the slit edges.

The ACE imager data are used to determine the location of the Sun's center. The intensity in the image center appears as a plateau, so the boundary of the Sun is identified by constructing a contour line at 15% of the maximum intensity (the 15% threshold was empirically determined) and fitted with an ellipse.

The locations of the slits on the Sun are found using the sun scans and the corresponding images. Figures 5a and 5b indicate the positions of the sun centres (solid dots) determined by the elevation scans from MAESTRO UV and Visible-NIR spectrometer data, along with the simulated sun boundaries using an ellipse model (solid large ellipses) applied to the ACE NIR Imager data. Each pixel represents a 0.013° field of view. Since the raw images' axes are fixed at 55.5° relative to the Earth's horizon (Gilbert et al., 2007), for straightforward interpretation, the images, along with the slits, are rotated so

https://doi.org/10.5194/egusphere-2025-4636
Preprint. Discussion started: 14 October 2025

that the X-axis is parallel to the Earth's horizon. However, it is important to note that the elevation and azimuth scans are only approximately parallel to the imager's X- and Y-axes.

Using the sun-scans and ACE Imager data, two solid lines are created, representing the MAESTRO UV and Visible-NIR slits. From the azimuth scan, the positions of the half maximum from the UV and Visible-NIR scan data are identified as the endpoints of each slit, marked as squares along with the dashed circles. The slit positions identified during pre-launch ground tests at DFL are the dashed lines.

https://doi.org/10.5194/egusphere-2025-4636
Preprint. Discussion started: 14 October 2025

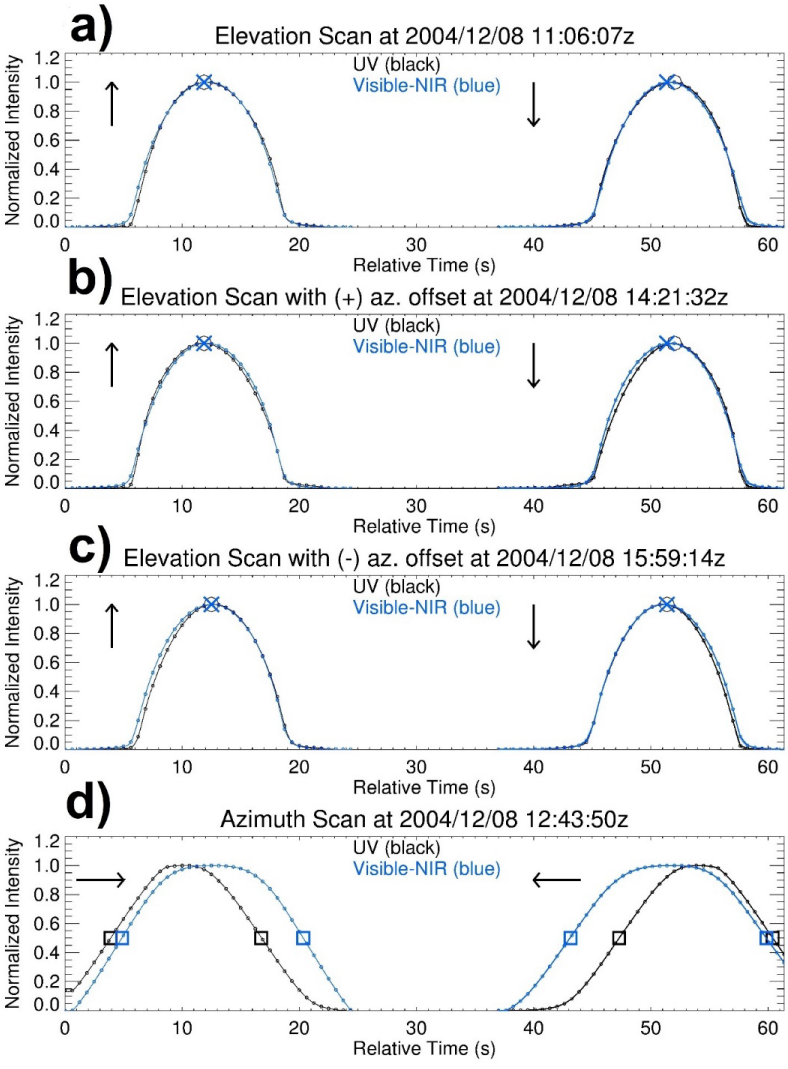

Figure 4: From the top, the integrated intensities from the MAESTRO UV (black) and Visible-NIR (blue) spectra recorded during an elevation scan (a), elevation scans with positive (b) and negative (c) azimuth offsets, and an azimuth scan (d). The maximum intensities during the elevation scans are marked with an "x" for UV and a circle for Visible-NIR. Half-maximum intensities during the azimuth scans are marked with squares. The vertical arrows indicate upward and downward elevation scans, while the horizontal arrows indicate azimuth scans to the left and right.

https://doi.org/10.5194/egusphere-2025-4636
Preprint. Discussion started: 14 October 2025

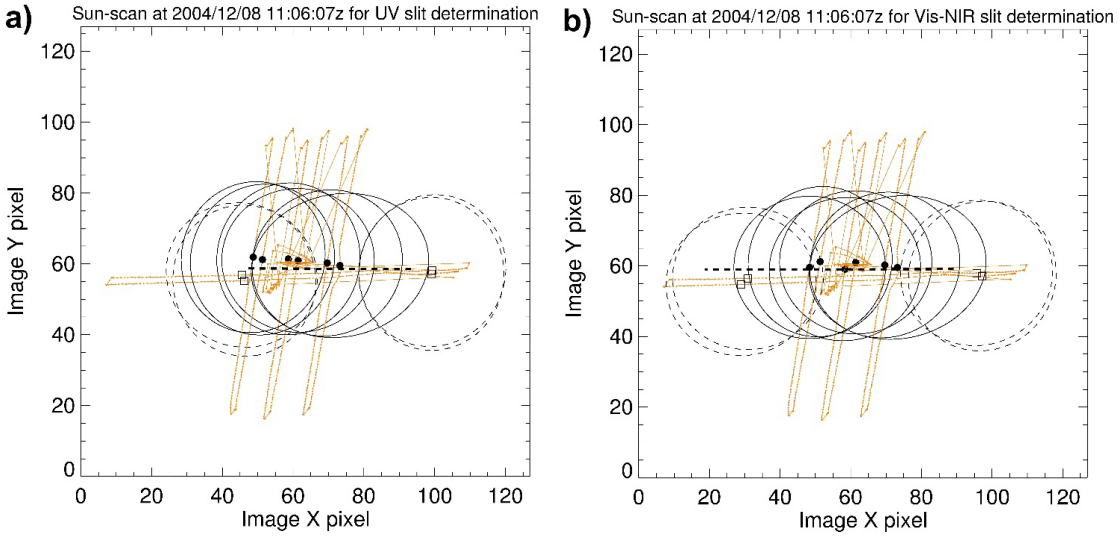

Figure 5 The elevation and azimuth sun scans recorded on 8 December 2004 (solid straight lines) associated with the MAESTRO UV (a, left panel) and Visible-NIR (b, right panel) spectrometers. The sun centres (solid dots) and boundaries (solid ellipses) on the ACE NIR Imager are derived at the time when the UV and Visible-NIR slits cross the sun centre during elevation scans. During azimuth scans, the sun centres (open squares) and sun boundaries (dashed ellipses) are determined from the time of the half maxima of UV and Visible-NIR intensities. The dashed straight lines represent the positions of the UV and Visible-NIR slits estimated from the pre-flight test at DFL.

Figure 6 shows the points on the UV and Visible-NIR slits estimated from the six sets of sun scans conducted in December 2004, the pre-launch tests at DFL, and the ACE-FTS FOV determined during the on-orbit commissioning (Walker et al., 2004). The slits from the DFL test are nearly parallel to the Earth's horizon and are slightly below the centre of the ACE-FTS FOV, which is close to the Sun's centre. For the on-orbit results, the Visible-NIR slit is almost horizontal and centred on the Sun, while the UV slit is slightly rotated clockwise, indicating that the FOV is about 0.04°, larger than the expected

https://doi.org/10.5194/egusphere-2025-4636
Preprint. Discussion started: 14 October 2025

280 0.022°. It is also shifted in the azimuth (to the right in Fig. 6) so that the slit does not encompass the Sun, indicating that as the satellite moves in elevation during an atmospheric scan, errors will arise in the normalized spectra. The in-flight measurements are elevated by about 0.026° from the pre-launch DFL tests, but the two spectrometers are aligned in elevation, passing through the ACE-FTS FOV.

These slit estimates in elevation and azimuth are somewhat imperfect, which might impact
285 retrievals, particularly at lower altitudes, as discussed in Sect. 3.3. However, it appears that the MAESTRO slits only changed slightly through launch.

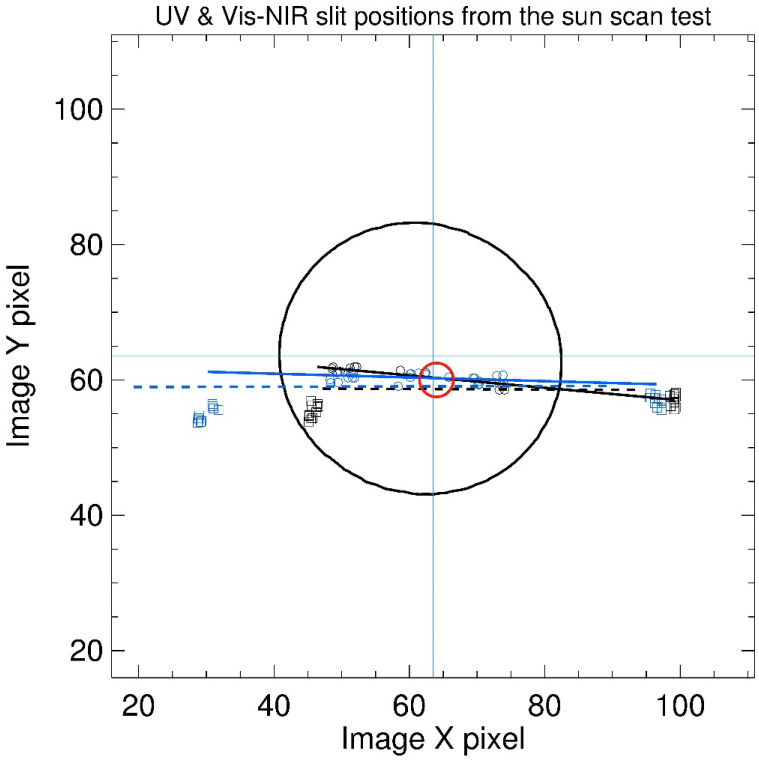

Figure 6: The MAESTRO UV (solid black line) and Visible-NIR (solid blue line) slits estimated from
290 six sets of sun-scans recorded in December 2004. This plot is an image of 96 x 96 pixels, cropped from the central part of the original 128 x 128 pixel image. The circles are the sun centres determined during

https://doi.org/10.5194/egusphere-2025-4636
Preprint. Discussion started: 14 October 2025

the elevation scans for both UV (black) and Visible-NIR (blue) spectrometers. The squares represent the sun centres obtained from the azimuth scans for the UV (black) and Visible-NIR (blue) slits used to determine the edges of the slits. The UV (dashed black line) and Visible-NIR (dashed blue line) slits, as estimated from pre-launch tests at DFL, are shown. The red circle is the ACE-FTS FOV, as determined from an early commissioning test. The solid black circle denotes the position of the sun's boundary.

3.3 The MAESTRO fields of view on the solar disk during occultation

During each occultation, the sun tracker is locked onto the sun centre by a quadrant sensor allowing the ACE Imagers to record solar images while ACE-FTS and MAESTRO take measurements. During sunset (sunrise), the tangent height decreases (increases), and the apparent solar disk shifts due to refraction, but the sun tracker keeps the instruments pointing at the radiometric centre of the Sun. However, at very low tangent heights, the sun image becomes compressed and asymmetric in the elevation direction, and the lower portion compresses more than the upper portion. Figure 7 presents a set of sun images captured by the ACE NIR Imager at tangent altitudes of approximately 100 km (Fig. 7a), 20 km (Fig. 7b), 15 km (Fig. 7c), and 10 km (Fig. 7d) during the sunset occultation measurement ss64172. The MAESTRO UV and Visible-NIR slits, derived from the DFL test (Fig. 6), are superimposed onto the solar disk. For uncertain reasons, the solar disk in the NIR image at high solar elevation is not quite a perfect circle (Fig. 7a) (Gilbert et al., 2007) with the ratio of the minor to major axes at about 0.95 when fitting the sun boundary to an ellipse (Fig. 8b).

In theory, for the Level 1 transmittance calculation, all measurements must originate from the exact same location on the Sun's disk. However, the MAESTRO slits do not precisely align with the tracker in elevation, and coupled with the flattening of the solar disk, a correction is required.

https://doi.org/10.5194/egusphere-2025-4636
Preprint. Discussion started: 14 October 2025

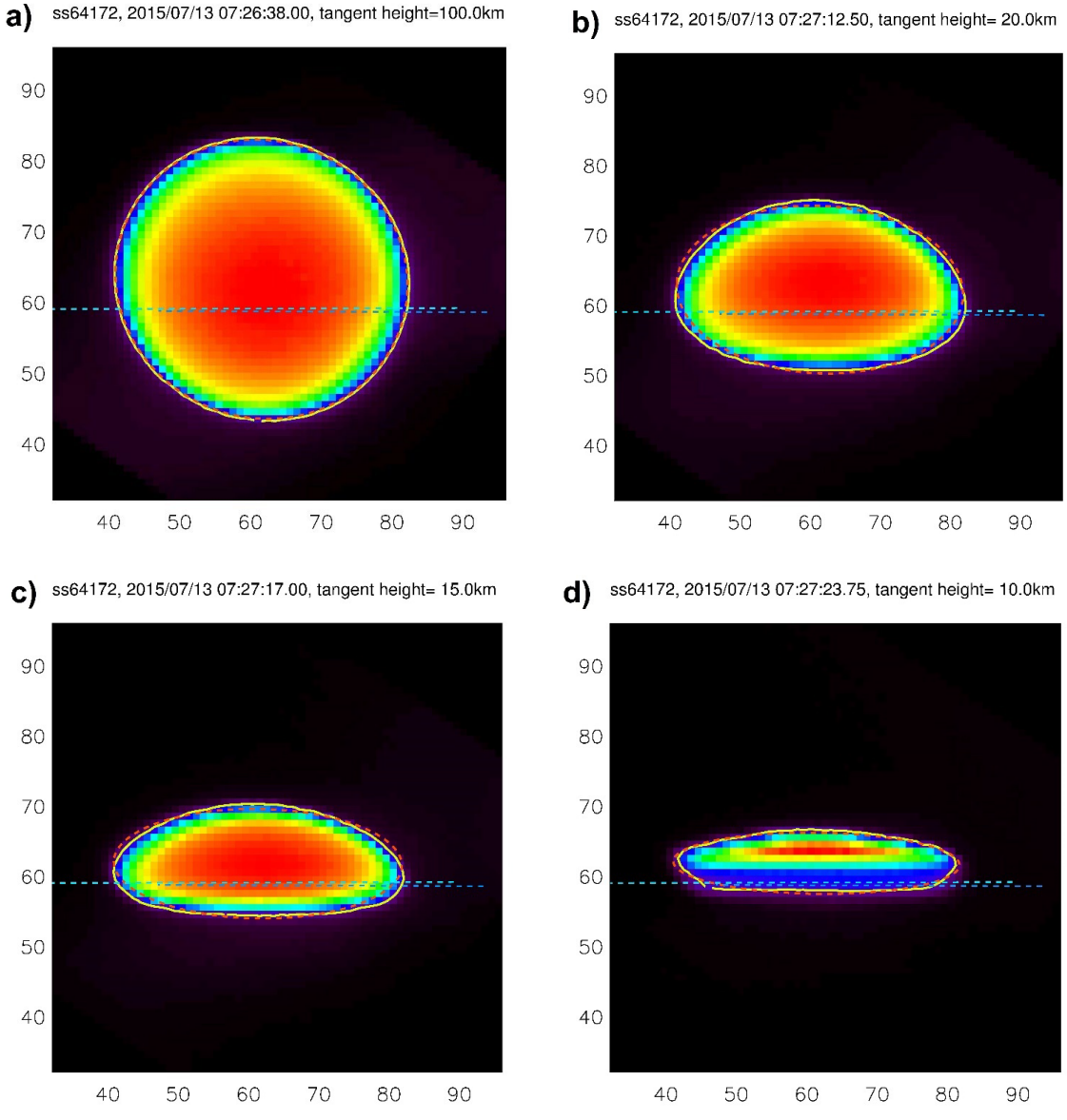

315

Figure 7 Sun images for ss64172 captured by the ACE NIR Imager at tangent altitudes of 100 km (a, top left), 20 km (b, top right), 15 km (c, bottom left), and 10 km (d, bottom right) for ss64172. The yellow contour represents 15% of the peak intensity, marking the Sun's boundary, and is fitted with an

https://doi.org/10.5194/egusphere-2025-4636
Preprint. Discussion started: 14 October 2025

ellipse (red). The UV (blue dashed line) and Visible-NIR (light blue dashed line) slits, obtained from the pre-launch DFL test (Fig. 6), are superimposed.

Following the procedure used in Sect. 3.2, a Sun boundary is established at 15% of the peak intensity of the image contour, and an ellipse model is used to determine the Sun's centre. Figure 8 illustrates the analysis of these derived parameters for ss64172. Figure 8a shows the ACE-FTS tangent height versus time curve for this occultation, with measurement times at tangent heights of 50 km, 30 km, 20 km, 15 km, and 10 km indicated by the dotted vertical lines. After reaching the position denoted by the vertical blue line, which is determined from when the standard deviation of the Sun's vertical coordinates drastically increases, the sun tracker unlocks. Figure 8b shows the ratio of the minor to major axes for the derived ellipse. Outside the atmosphere, the ratio is ~0.95, but within the atmosphere, the disk becomes distorted below ~35 km and then progressively appears more "squashed" as the ratio decreases.

Figure 8c and 8d show the azimuth (X) and elevation (Y) midpoints of the sun's edges. The azimuth midpoint (Fig. 8c) is almost constant until the tracker loses lock. Below about 50 km the elevation midpoint trends downward (Fig. 8d) as the sun tracker follows the centre of the radiance. This centre is a fixed location on the Imager, but itself not at the midpoint of the ellipse contour. Figure 8e shows the orientation angle of the major axis with respect to the X-axis, reflecting the roll of the spacecraft. At high altitudes, the sun image is a near perfect circle, but the orientation angle is around -20° due to the imperfect imaging of the sun disk. Below 50 km and before the tracker loses lock, the non-circular image asymptotes to zero orientation angle.

https://doi.org/10.5194/egusphere-2025-4636
Preprint. Discussion started: 14 October 2025

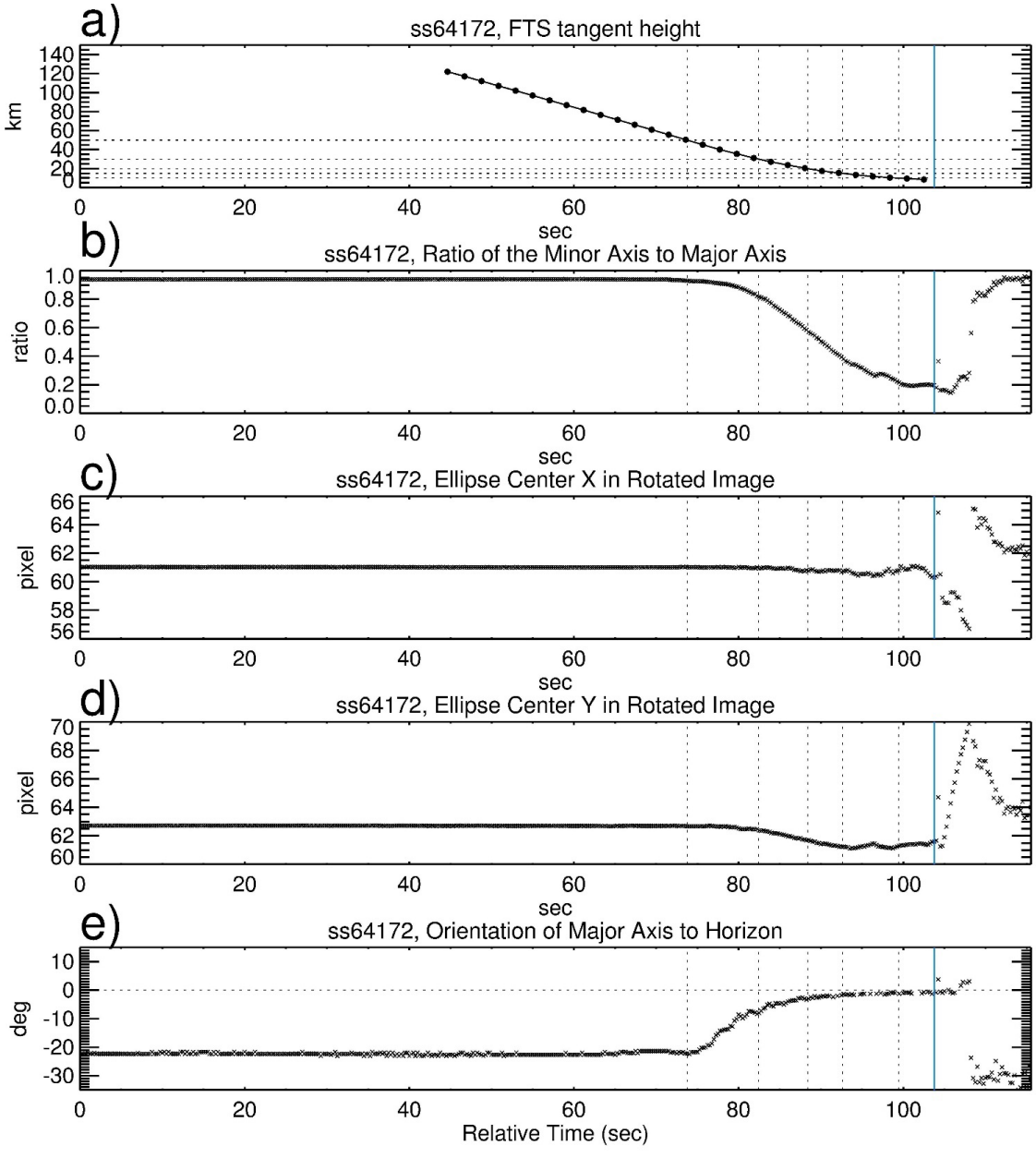

Figure 8 The ACE-FTS tangent height vs. time curve for ss64172 (a, top). Time sequences of the ratio of the minor to major axes (b, 2nd row), the sun centre's X- and Y-coordinates in the images (c and d; 3rd and 4th row), and the orientation angle of the major axis to the horizontal axis (e, bottom). Vertical

https://doi.org/10.5194/egusphere-2025-4636
Preprint. Discussion started: 14 October 2025

dotted lines indicate the time for ACE-FTS measurement tangent heights at 50 km, 30 km, 20 km, 15 km, and 10 km. The vertical blue lines indicate the time at a low altitude when the sun tracker is no longer locked on the Sun.

Figures 9a and 9b show the transmittance profiles estimated from the ACE NIR Imager intensities integrated along the MAESTRO UV and Visible-NIR slits derived from both the DFL test and the 8 December 2004 in-flight sun scan test, respectively. The Imager transmittances calculated from the ACE-FTS FOV (see 3.2) are co-located and overplotted as the reference. The transmittance profiles through the slits, derived from the in-flight sun scan test, closely align with the reference profile. At altitudes below about 15 km, the DFL slit-position-derived transmittance is lower than that of the reference profile, with the ratios between the two transmittance profiles reaching about 50 % around 11 km. The MAESTRO Level 1 transmittance data is underestimated at low altitudes for all wavelengths when compared to other solar occultation instruments, e.g., SAGE III/ISS (not shown here). This is more consistent with the DFL ratio than that from the in-flight tests. Although only one wavelength is investigated here, this study provides a clue for understanding the possible underestimation of MAESTRO nominal transmittances. Further exploration of this topic is necessary but falls beyond the scope of this study.

https://doi.org/10.5194/egusphere-2025-4636
Preprint. Discussion started: 14 October 2025

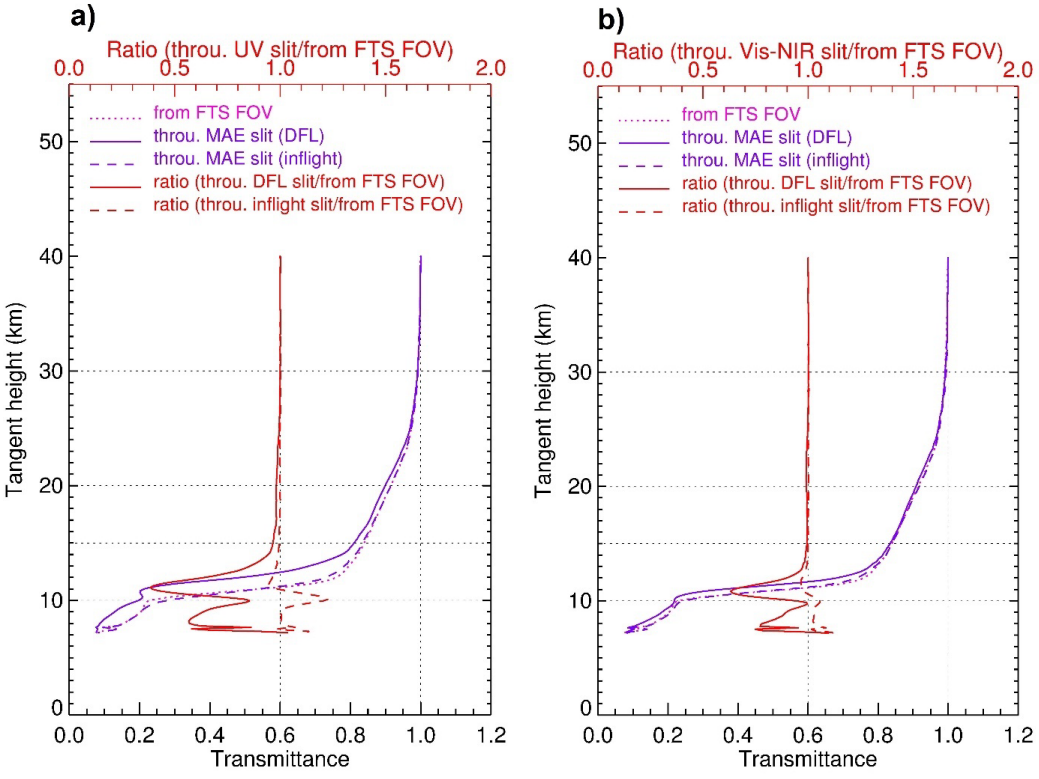

Figure 9 The transmittance profiles below 40 km derived from the ACE NIR Imager integrated intensities alongside the MAESTRO UV (a, left panel) and Visible-NIR slits (b, right panel) estimated from the DFL test (solid blue) and from the in-flight sun-scan test (dashed blue), as well as the transmittance profile derived from the ACE NIR image intensities on the pixels where the ACE-FTS FOV is located (dotted pink). The two red curves are the ratios (top scales) of the DFL slit-position-derived transmittances (solid red) and the in-flight sun scan test slit-position-derived transmittances (dashed red) to the ACE-FTS FOV-derived transmittances.

3.4 Instrument temperature monitoring and anomaly assessment

Figure 10 shows a typical short-term (48 hours) temperature plot for 3-4 March 2024 for the radiator (Fig. 10a), the diffraction grating of the Visible-NIR spectrometer (Fig. 10b), and the electronics board

https://doi.org/10.5194/egusphere-2025-4636
Preprint. Discussion started: 14 October 2025

(Fig. 10c). The radiator is at the lowest temperature, about -9°C, the spectrometer grating is about -6.5°C, and the electronics board is at about 20°C. The orbital timescale is the dominant pattern, with a cycle from sunset to sunrise at about 3°C for the radiator, 0.5°C for the grating, and 1.5°C for the electronics. The electronics temperature (Fig. 10c) exhibits additional changes around sunset and sunrise due to occultation measurement activities.

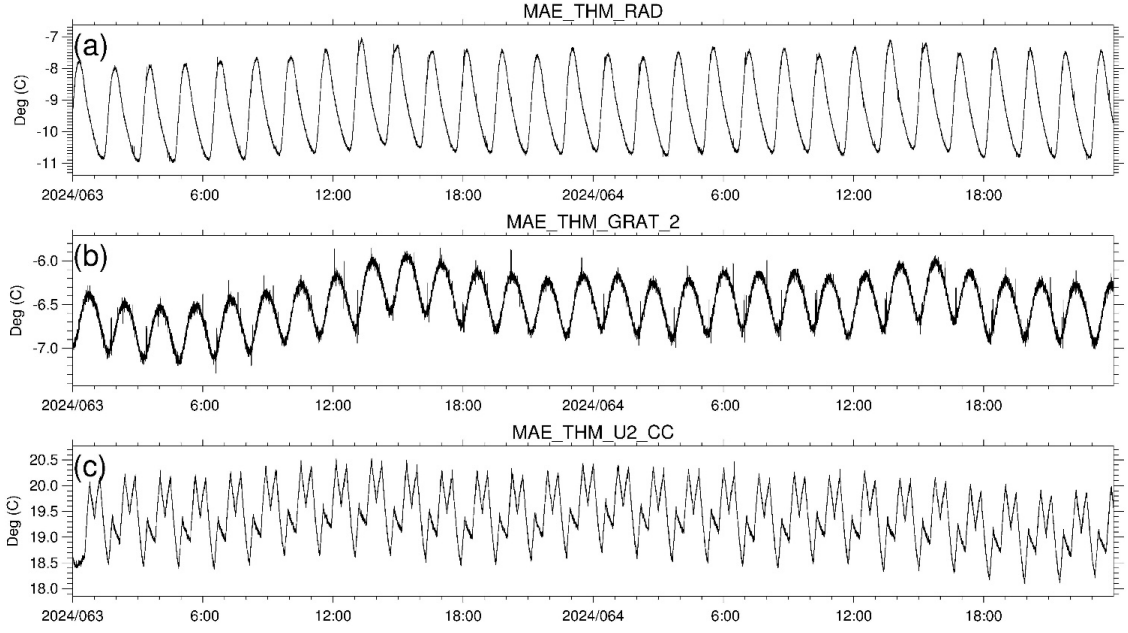

Figure 10 48-hour temperature (°C) for 3-4 March 2024 for the radiator (a, top), the grating for the Visible-NIR spectrometer (b, middle), and the electronics board (c, bottom).

Figure 11 shows a longer-term (1 year) temperature plot for the Visible-NIR spectrometer grating only. Temperature variations are influenced by multiple factors, including month-to-month changes (about 2°C) due to the approximately 4-month beta angle cycle and the annual cycle of the Earth-Sun distance. The features in June and December result when the satellite is exposed to prolonged sunlight for more than two weeks at high beta angles (>60°) when no occultation measurements are possible. At

https://doi.org/10.5194/egusphere-2025-4636
Preprint. Discussion started: 14 October 2025

that time, MAESTRO only makes high sun measurements. While in early July, the temperature drops when the ACE-FTS undertakes decontamination for a few days, and no measurements are taken. Other temperature telemetry records (not shown) display similar patterns but at different magnitudes. Periodic temperature variations occur throughout the mission.

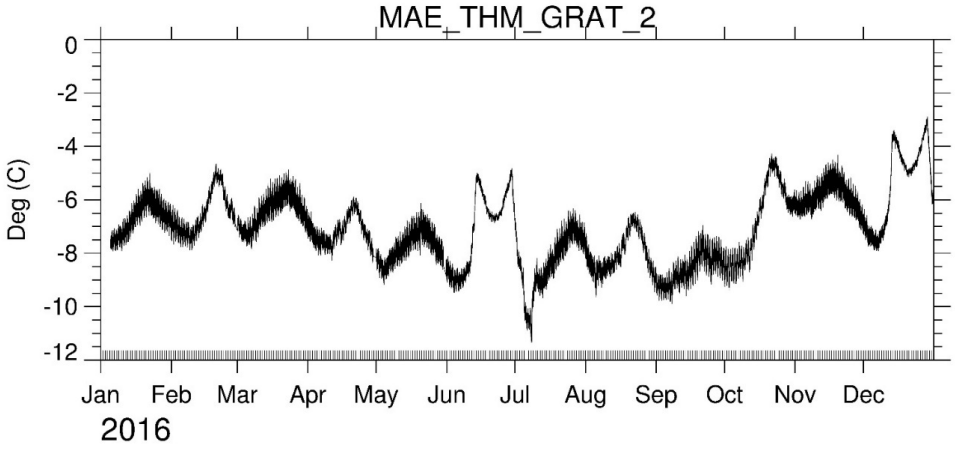

Figure 11 One-year temperature record for the grating of the Visible-NIR spectrometer.

Figure 12 presents the 21-year temperature history for the Visible-NIR spectrometer grating. The faster cycles are superimposed on a long-term record that is generally stable. However, there are two notable exceptions: 1) the increase in temperature between September 2009 and September 2010, which has no apparent cause, and 2) the persistent decrease of about 5°C starting 17 June 2015, when the star tracker failed, leading to reduced power consumption for the satellite. The temperature changes of the gratings affect the wavelength assignment for the detector pixels, which will be addressed in Sect. 3.5.2. This anomaly has allowed us to probe several issues, which are discussed in Section 3.5.

https://doi.org/10.5194/egusphere-2025-4636
Preprint. Discussion started: 14 October 2025

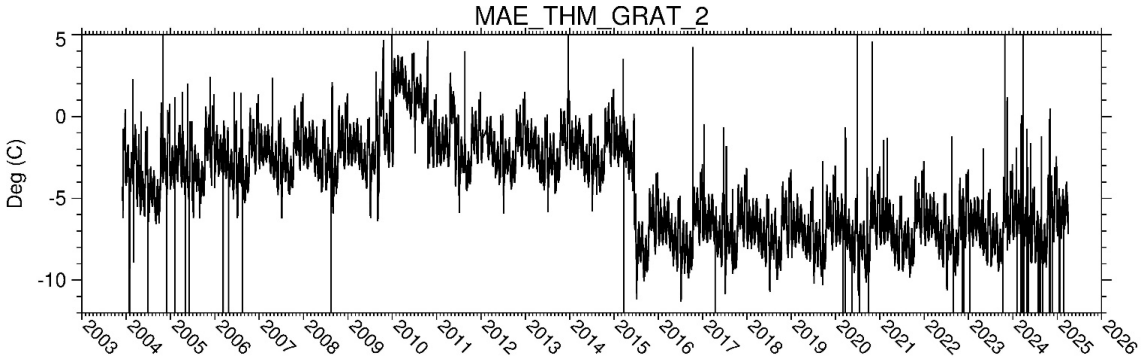

405 **Figure 12** The temperature history for the Visible-NIR spectrometer grating 2004-2025.

3.5 Impact of star tracker failure on the MAESTRO performance

3.5.1 Impact on the satellite orientation

410

The satellite's primary attitude control is through a 3-axis stabilization system, consisting of a momentum wheel, torque rods along three axes, one fine and six coarse sun sensors, and a magnetometer (Dahl et al., 1999). Pointing control provides a precision of ±1° in the pitch and yaw axes (3σ) and ±2° in the roll axis (3σ) (EO Portal, 2025). Secondary roll control was provided by a star

415 tracker, which failed on 17 June 2015.

The star tracker failure had the potential to modify the MAESTRO slits' location on the sun disk by causing variations in the satellite's roll. The sun images allow us to look for potential changes around this failure. As discussed in Sect. 3.3, the sun image becomes distorted as the tangent altitude decreases; however, if the spacecraft's roll changes, the image's rotation will change. Figure 13 shows scatter plots

420 of the orientation angle of the solar disk and the ratio between the minor and major axes of the ellipse fitted to sun images in July and August for both 2014 (before the failure) and 2015 (after the failure). The ratio reflects the satellite's tangent height; the smaller the ratio, the lower the height. Using the months of July and August, rather than immediately before and after the failure, provides a consistent

https://doi.org/10.5194/egusphere-2025-4636
Preprint. Discussion started: 14 October 2025

environment for comparison. Spacecraft rotations would be visible if there were differences between the two years.

Given that the projection of the slits on the Sun, which has a diameter of 0.5° (40 pixels on the Imager), is nominally 0.022° (elevation) x 0.65° (azimuth) for the UV and 0.022° x 0.89° for the Visible-NIR channel (McElroy et al., 2007), a 1° rotation of the spacecraft implies that the slit is smeared in elevation by approximately 0.0087° or 0.49 km (1 pixel is approximately 0.7 km; Gilbert et al., 2007). Figures 13a-d highlight the differences between 2014 and 2015 by fitting lines within the ratio range of 0.15−0.6 (corresponding to altitudes of 10-20 km) and comparing the resulting lines of best fit. July has fewer data points than August due to scheduling conflicts with the annual ACE-FTS detector decontamination. Apart from outliers, all the data within the 0.15−0.6 ratio range falls between +1° and -3°, which implies that the slit smearing from this issue is less than 1.5 km at most.

Additionally, only negligible differences are found between the data obtained before and after the star tracker failure. The largest difference between the pre- and post-failure data occurs for the July sunrise observations, with a change that is still less than 0.5°. Therefore, the difference in rotation between the two periods is much less than other factors; instead, the primary feature is the change from high to low altitudes, and the effect of the failure on rotation is minimal. There is a slope from high to low altitudes the assessment of which will be incorporated into a future study.

https://doi.org/10.5194/egusphere-2025-4636
Preprint. Discussion started: 14 October 2025

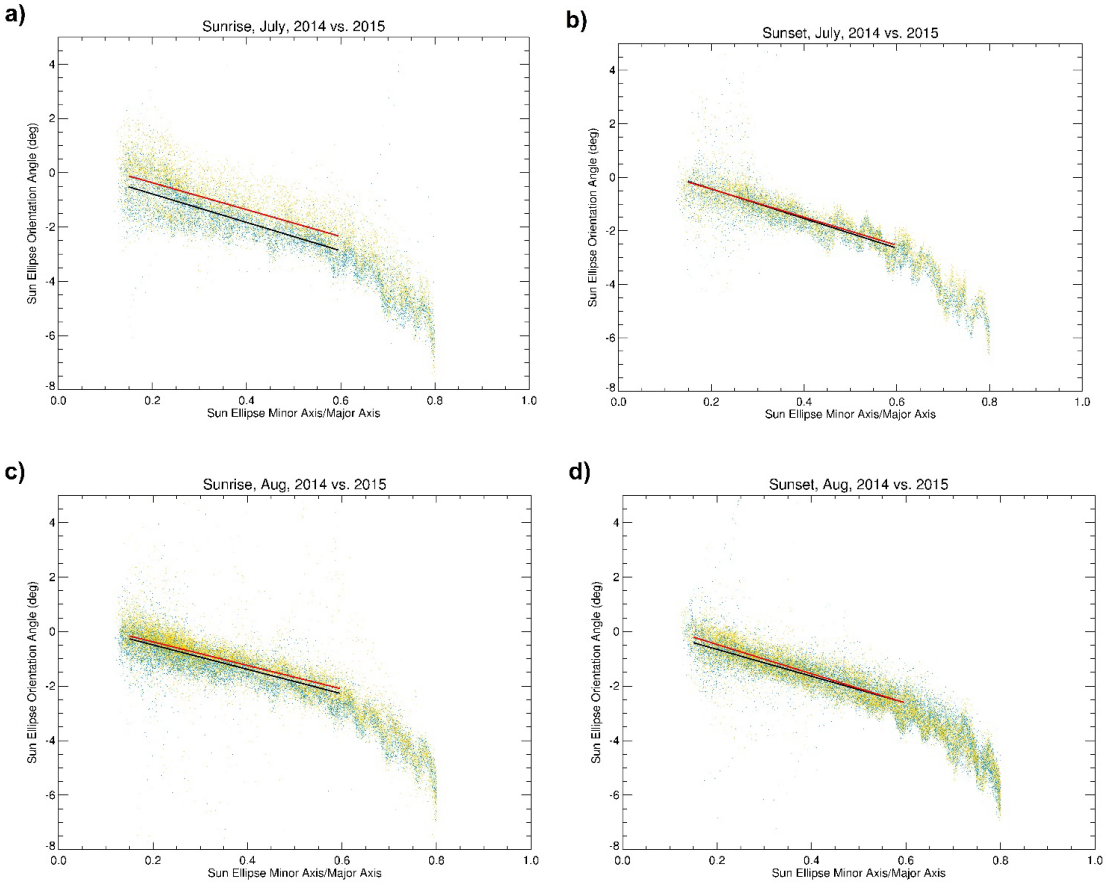

Figure 13 Scatter plots showing the orientation angles of the major axis of the simulated sun and the ratios of the minor and major axes of the ellipse before the star tracker failure (2014, light blue dots) and after the failure (2015, orange dots) for July sunrise (a), July sunset (b), August sunrise (c) and August sunset (d) measurements. The black (2014) and red (2015) lines are the respective linear fits for the 2014 and 2015 data points within the ratio range of 0.15−0.6. The plots were cut off below 0.15 due to the sun tracker losing its lock on the Sun at low altitudes, and above 0.8, as the images are almost circular. ACE NIR Imager data from July have fewer data points than the August data, as the ACE-FTS detector decontamination is typically done during early July, and thus, no occultation measurements are made.

https://doi.org/10.5194/egusphere-2025-4636
Preprint. Discussion started: 14 October 2025

Sporadic outliers mainly originate from images taken at low altitudes when the sun tracker fails to lock onto the sun, resulting in indeterminate data.

3.5.2 Impact on the wavelength assignment

There is a known dependency of the MAESTRO wavelength on temperature, which the data processor addresses. This processor fits the high sun reference spectrum for an occultation to a smoothed high-resolution Fraunhofer solar spectrum (Chance et al., 2010), convolved with the MAESTRO instrument line shape using a high-order polynomial model. The polynomial fit is then used as a reference for the wavelength assignment for each occultation spectral measurement with the adjustment of shift, stretch and possibly higher order terms. Normally, the effect of a temperature change within an occultation is small, and the effect of temperature variations between orbits is readily considered with this approach.

The star tracker failure in 2015 affected the wavelength assignment due to the temperature change in the spectrometer grating (see Fig. 12). Figure 14a displays the raw optical depth spectra collected at various tangent heights (93, 51, 35, 30, 25, 21, and 18 km) for pixels 300 to 600 of the Visible-NIR spectrometer before (8 June 2015) and after (9 July 2015) the star tracker failure. Shifts in the spectrum are especially apparent between pixels 490-497, particularly at lower altitudes. Figure 14b illustrates the differences between the spectra before and after the star tracker failure, highlighting the wavelength shift. Fig. 14c shows the same data as Fig. 14a, but with wavelengths assigned by the processor, and Fig. 14d shows the differences between the wavelength assignment from before and after the star tracker failure. These differences are significantly less than those in Fig. 14b, thereby demonstrating this approach's effectiveness even with a large temperature deviation. Thus, while not designed to handle the large temperature shift caused by the star tracker failure, this anomaly allows for an on-orbit

https://doi.org/10.5194/egusphere-2025-4636
Preprint. Discussion started: 14 October 2025

475 confirmation of the data processing algorithm. Given the periodic temperature variations (see Sect. 3.4), it shows that the effect of the wavelength shifts is taken into account.

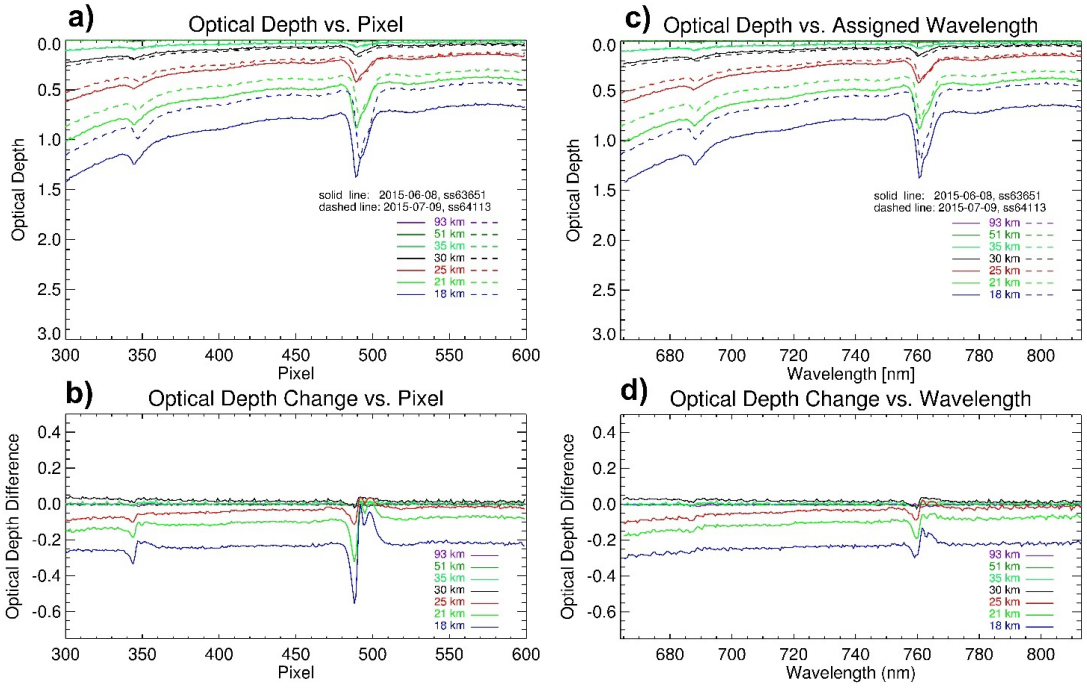

Figure 14 The Visible-NIR optical depth spectra taken at several tangent heights (93, 51, 35, 30, 25, 21, 480 and 18 km) during sunset occultation ss63651 on 8 June 2015 before the star tracker failure (solid) and during ss64113 on 9 July 2015 after the star tracker failure (dashed) as a function of pixel number (a, top left) and their differences (b, bottom left). The same spectra but with assigned wavelengths (c, top right) and their differences (d, bottom right).

485 **3.6 Long-term trends in the UV and Visible-NIR high sun spectra**

Figures 15a and 15b show the trends in the UV and Visible-NIR high sun spectra from 2004 to 2025, with one spectrum plotted per year. Part of the UV spectrum overlaps with the Visible-NIR, allowing for

https://doi.org/10.5194/egusphere-2025-4636
Preprint. Discussion started: 14 October 2025

a direct comparison between the two spectrometers. MAESTRO trace gas retrievals use the region from 420−545 nm for UV NO_2 and O_3, and from 530-755 nm for Visible-NIR O_3 with the temperature-dependent absorption cross-sections taken from the GOME flight model (Burrows et al., 1998, 1999). Figures 16a and 16b show the normalized time series of high sun spectral intensities at wavelengths 440 nm, 490 nm, 530 nm (arbitrarily chosen for UV) and 530 nm, 603 nm, 675 nm, 779 nm, 875 nm, and 1012 nm (the same wavelengths used for retrieving the Visible-NIR aerosol data).

The UV spectrometer at 440−490 nm intensity decreases rapidly from the launch values to a 90% reduction by 2006 for 440 nm and 2010 for 480 nm. After 2022, the UV spectrometer signal shows a gradual recovery of about 10−40% by 2025, with no definitive cause. However, this increased signal may allow for the retrieval of NO_2 and O_3 profiles in the future. The Visible-NIR spectrometer wavelengths exhibit different trends: longer wavelengths are more stable over time, while shorter wavelengths follow similar trends to the UV spectrometer at the same wavelength. Since they are from separate spectrometers but share common input optics, these decreasing trends are likely associated with the optics outside of the MAESTRO instrument.

Because solar occultation measurements are self-calibrating, the nearly simultaneous measurements of high sun and occultation spectra do not require the exact knowledge of the instrument's responsivity for transmittance calculation (McCormick et al., 1989; McElroy et al., 2007), allowing for the compensation of instrument changes. The Visible-NIR spectrometer continues to provide valid retrievals throughout the mission; however, due to the degradation of UV spectra, the UV NO_2 and O_3 data are not valid after December 2009 (Jeffery et al., 2025). However, if the UV spectra continue to recover, retrievals from this channel will be resumed.

https://doi.org/10.5194/egusphere-2025-4636
Preprint. Discussion started: 14 October 2025

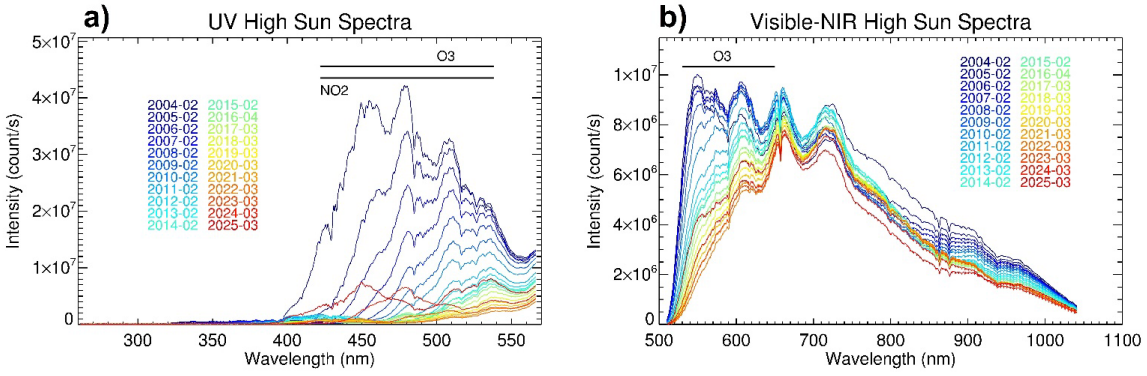

Figure 15 A series of reference exo-atmospheric spectra obtained from the MAESTRO UV spectrometer (a, left) and the Visible-NIR spectrometer (b, right) covering 2004–2025, with one spectrum shown yearly. The relevant wavelength bands for the UV NO_2, O_3, and Visible-NIR O_3 retrievals are indicated by horizontal lines near the top of the plots.

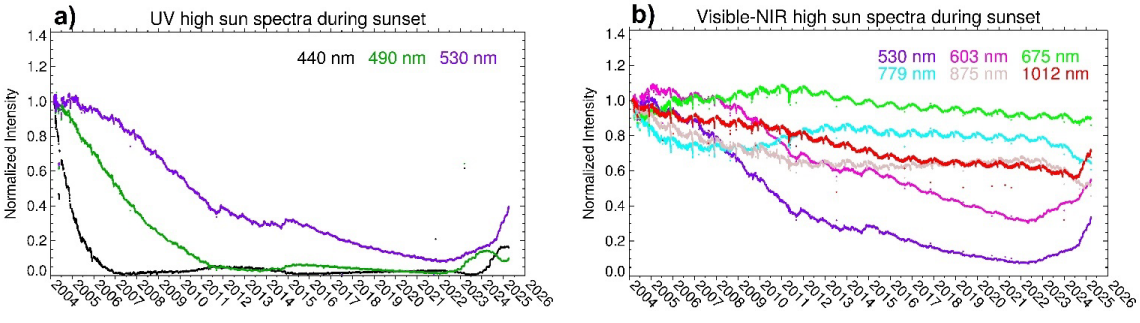

Figure 16 Normalized time series of high sun spectral intensities between 2004–2025 from the UV spectrometer (a) and Visible-NIR spectrometer (b).

3.7 Determination of MAESTRO tangent heights

The initial plan for the MAESTRO retrievals was to utilize the time-tagged ACE-FTS pressure and temperature (p, T) profiles, along with the MAESTRO data. However, it was found early in the mission that the time from MAESTRO was inconsistent with that of ACE-FTS, likely due to variability in the

https://doi.org/10.5194/egusphere-2025-4636
Preprint. Discussion started: 14 October 2025

interrupt latency of the satellite bus computer (McElroy et al., 2007). Additionally, despite the on-orbit measurements discussed in Sect. 3.2, there is uncertainty between the MAESTRO and ACE-FTS FOVs and, thus, differences in the line-of-sight (LOS). Therefore, the retrieval algorithm must consider the time difference, UV LOS angle, and Visible-NIR LOS angle together.

In MAESTRO v1.2 data (Kar et al., 2007), these three parameters were set to constant values for all measurements, adjusting them until an ensemble of MAESTRO NO_2 and O_3 data agreed with those from ACE-FTS. At UTC (Coordinated Universal Time) times later than 20:00z, MAESTRO profiles were found to often be larger than those from ACE-FTS by a factor of approximately 1.5−2. At all other times, MAESTRO agreed with ACE-FTS, suggesting that the time shift between MAESTRO and ACE-FTS depended on UTC.

Later retrieval versions calculated the time shift for each measurement. In v3 (and sub-versions thereof), the time shift for Visible-NIR measurements varied for each measurement, and the FOV angle was set to zero. The Visible-NIR A-band O_2 slant column was fitted to the ACE-FTS air density by adjusting the time shift. In this process, a global scaling factor was introduced to link the two quantities, as it should be a constant. In practice, two scaling factors were required, one for sunset and the other for sunrise, which were empirically determined through ensemble comparisons of MAESTRO and ACE-FTS observations, typically of data from 2005−2006 when both action tables “A” and “B” are used. For the UV channel, the same time shift was used as the Visible-NIR, and the angle for the UV LOS relative to the Visible-NIR was determined from a test of occultation ss2873. In v3.13, this process was specified by using four scaling factors for corresponding scenarios (sunrise/sunset and the action tables “A”/ “B”) which were only applied to the Visible-NIR O_3 and aerosol data products. Unfortunately, none of the v3 retrieval algorithms produced satisfactory data products for all UV NO_2, UV O_3 and Visible-NIR O_3 profiles simultaneously.

https://doi.org/10.5194/egusphere-2025-4636
Preprint. Discussion started: 14 October 2025

The current retrieval, version 4.5, assumes that the angle shift is, to the first order, equivalent to an additional time shift with opposing signs for sunset and sunrise, and reduces the number of parameters by fixing the angle shift to zero while using independent time shifts for the UV and Visible-NIR. The time shifts were determined by fitting the respective MAESTRO UV and Visible-NIR O_3 columns to the ACE-FTS O_3 columns.

To illustrate this, a subset of data was processed using two approaches. First, the Visible-NIR data from January to February 2006 were processed with a fixed time shift of -0.925 s and an angle of -0.011° (close to 1 pixel on an image, Sect. 3.2) for both sunset and sunrise. Figures 17a (sunset) and 17b (sunrise) show the Visible-NIR O_3 mean profiles and standard deviations alongside those from ACE-FTS. Fig. 17c and 17d are the corresponding absolute and relative differences. There is good agreement between 22 and 50 km, with a <5 % difference for both sunset and sunrise measurements.

Then, the same subset of MAESTRO data was processed with a static time shift of -1.325 s for sunset and -0.5 s for sunrise and with the angle shifts all set to zero. The results are shown in Fig. 18. For sunset, the difference profiles in Fig. 17c and Fig. 18c show similar structures, and for sunrise, Fig. 17d shows a variation of <10 % and negative biases of between -8 % and -3 % between 20 and 50 km, while Fig. 18d shows variations of <10 % and altitude-dependent biases from -10 % to 10 % between 20 and 50 km. Thus, simplification with a time shift of -0.913-0.412 s for sunset and -0.913+0.412 s for sunrise with the angle shifts to zero gives comparable results to the more complex formulation. The tilt of profile differences (see Figs. 17c/d, 18c/d) may be attributed to the altitude-dependent underestimation of the MAESTRO transmittance and requires further investigations.

Retrievals for the UV spectrometer using v4.5 are similar, but independent from the Visible-NIR; fitting UV O_3 to ACE-FTS O_3 is used to derive the time shift for each occultation. Then the UV NO_2 and O_3 are retrieved simultaneously using that time shift.

https://doi.org/10.5194/egusphere-2025-4636
Preprint. Discussion started: 14 October 2025

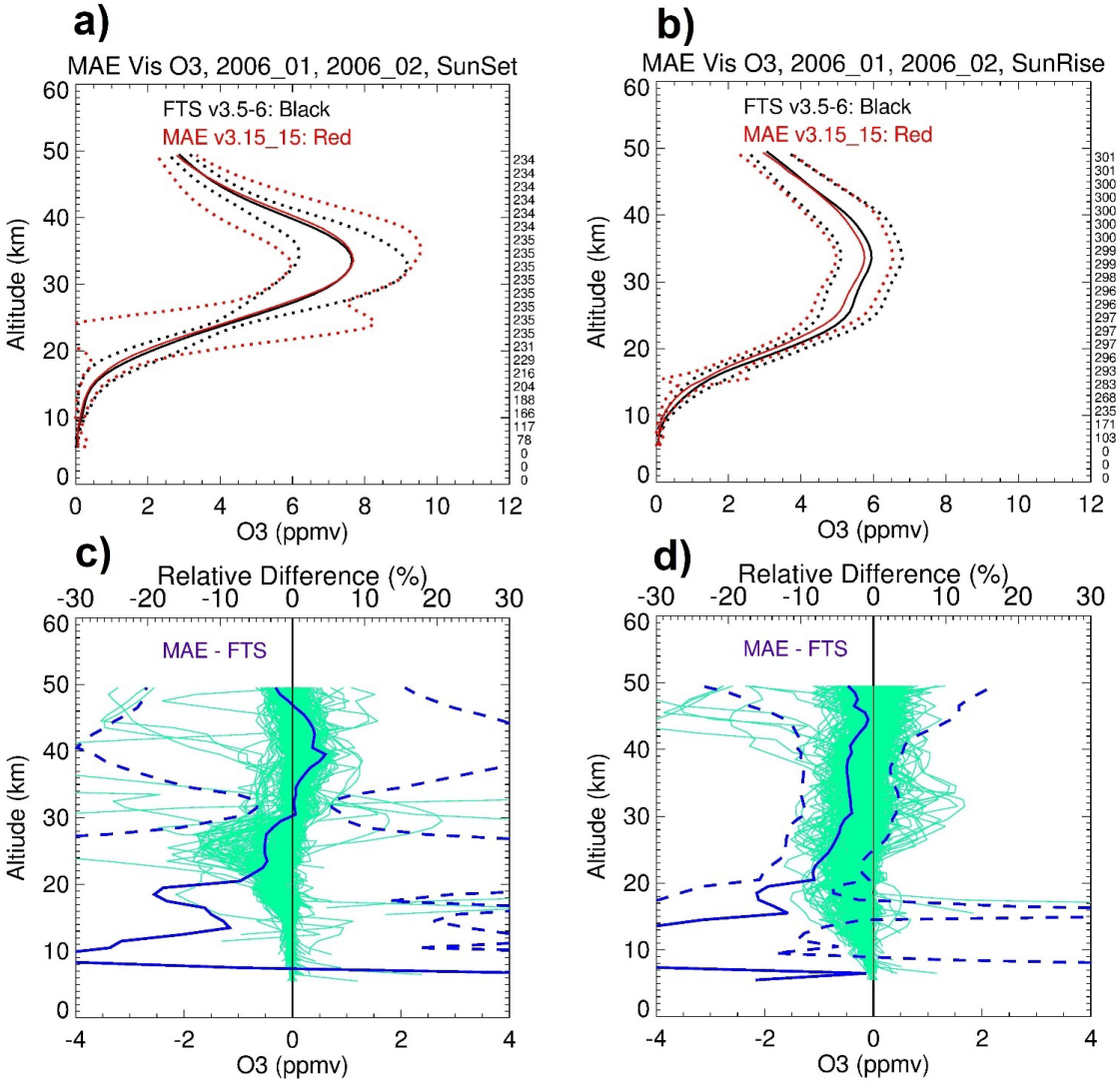

570

Figure 17 The mean O_3 profiles from MAESTRO (solid black) and ACE-FTS (solid red) averaged over January and February 2006, with a static time shift of -0.925 s, a fixed angle shift of -0.011° for both sunset (a, top left) and sunrise (b, top right) measurements along with their standard deviations (dotted black and dotted red lines). Absolute differences (MAESTRO – ACE-FTS, green lines; lower axes), the
575 mean relative differences (solid blue; upper axes), and their standard deviations (dashed blue; upper

https://doi.org/10.5194/egusphere-2025-4636
Preprint. Discussion started: 14 October 2025

axes) are shown for sunset (c, bottom left) and for sunrise (d, bottom right). The values along the right vertical axes in a and b show the number of data points compared at each altitude.

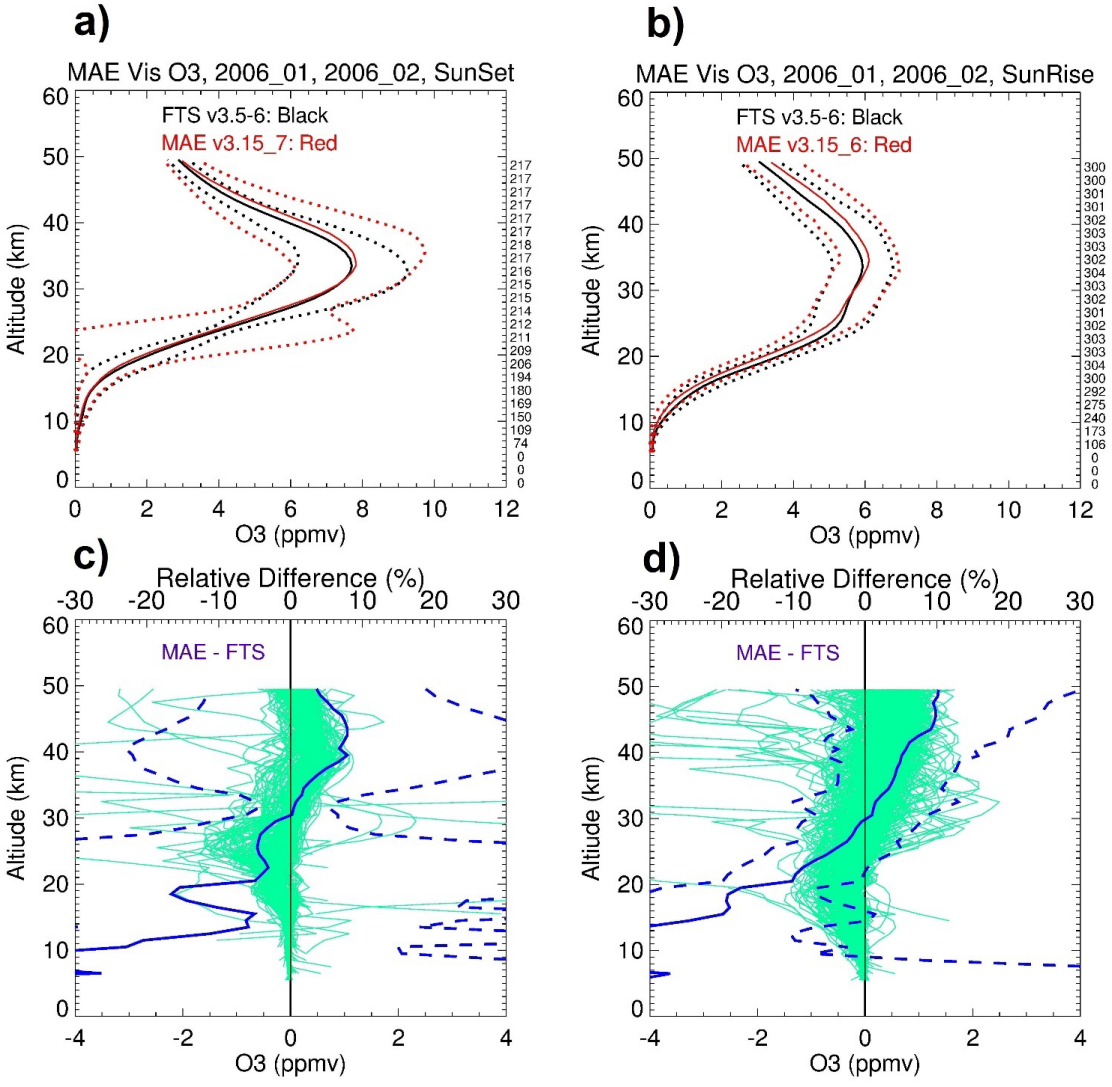

580 **Figure 18** Similar to Fig. 17, but with a static time shift of -1.325 s for sunset and -0.5 s for sunrise; the angle shifts are set to zero.

https://doi.org/10.5194/egusphere-2025-4636
Preprint. Discussion started: 14 October 2025

4. Conclusions

The MAESTRO instrument aboard the Canadian SCISAT satellite has been operating for over 21 years. It has produced one of the longest satellite records of UV-Visible-NIR measurements, invaluable for understanding atmospheric constituents with high vertical resolution. This paper addresses some of the key challenges in MAESTRO's operation and provides insight into how these issues have been resolved, including:

- The spectral intensities from the MAESTRO UV and Visible-NIR spectrometers have degraded over time. While intensity was degraded to 90% at shorter wavelengths during the first two years of the mission, wavelengths longer than 600 nm remain at greater than 50% of their initial intensity. Therefore, O_3 and aerosol measurements are available throughout the entire mission. Unexpectedly, a partial recovery of UV spectral signals began in 2022, with 10−40% of the initial intensity recovered by 2025. Preliminary retrievals appear to be viable but need a comprehensive analysis before dissemination.
- The current measurement scheme, set "B" of action tables, has not changed since August 2005 and effectively addresses the large dynamic range of incoming irradiances during an occultation.
- An unexpectedly fortuitous event, the failure of the star tracker, has allowed us to verify that the changes of wavelength registration caused by temperature changes are correctly determined by using a spectral fitting to both the high sun and occultation spectra that employs Fraunhofer lines.
- For MAESTRO retrievals to use the ACE-FTS pressure and temperature data, the variations between MAESTRO and ACE-FTS times, as well as an unknown set of angles between the MAESTRO and ACE-FTS LOSs, must be accounted for. This paper presents a solution that

https://doi.org/10.5194/egusphere-2025-4636
Preprint. Discussion started: 14 October 2025

fits MAESTRO UV and Visible-NIR O_3 profiles to ACE-FTS O_3 profiles separately by adjusting two independent time shifts, one for each spectrometer, while setting the angle shifts to zero. The success of this approach is demonstrated for low- and middle-stratosphere retrievals here, as well as in Jeffery et al. (2025), who validated the MAESTRO v4.5 NO_2 and O_3 data.

- An ongoing area of research is the MAESTRO retrieval at low altitudes, where refraction causes the Sun's image viewed by the ACE instruments to change shape, and consequently, the MAESTRO slits' position on the Sun to shift. We have utilized ACE Imager data, and the knowledge of the MAESTRO slit positions on the Imagers to demonstrate the issues. Further work on this will refine the retrievals for the lowest altitudes.

The MAESTRO instrument, together with the ACE-FTS, is expected to continue operations into the future.

Contributions of the authors: JZ performed the analyses and wrote the manuscript. TM is the project Principal Investigator (PI) and helped edit the manuscript. JD oversees the operation and data processing and helped edit and finalize the manuscript. KW managed the project and helped edit the manuscript. PJ helped edit the manuscript.

Competing interest. The authors declare that there are no conflicts of interest involved.

Acknowledgments

This study was funded by a contract from the Canadian Space Agency (CSA) as part of the Canadian-led mission - the Atmospheric Chemistry Experiment (ACE) supported by the CSA. The MAESTRO

https://doi.org/10.5194/egusphere-2025-4636
Preprint. Discussion started: 14 October 2025

instrument operation has been supported by the CSA's Satellite Operations Centre and the ACE Science Operations Centre (SOC) at the University of Waterloo. The MAESTRO instrument was developed and built by Environment and Climate Change Canada (ECCC) and EMS Technologies.

References

Bernath, P. F., McElroy, C. T., Abrams, M. C., Boone, C. D., Butler, M., Camy-Peyret, C., Carleer, M., Clerbaux, C., Coheur, P. F., Colin, R., DeCola, P., De Maziíere, M., Drummond, J. R., Dufour, D., Evans, W. F. J., Fast, H., Fussen, D., Gilbert, K., Jennings, D. E., Llewellyn, E. J., Lowe, R. P., Mahieu, E., McConnell, J. C., McHugh, M., McLeod, S. D., Michaud, R., Midwinter, C., Nassar, R., Nichitiu, F., Nowlan, C., Rinsland, C. P., Rochon, Y. J., Rowlands, N., Semeniuk, K., Simon, P., Skelton, R., Sloan, J. J., Soucy, M.-A., Strong, K., Tremblay, P., Turnbull, D., Walker, K. A., Walkty, I., Wardle, D. A., Wehrle, V., Zander, R., and Zou, J.: Atmospheric Chemistry Experiment (ACE): mission overview, Geophys. Res. Lett., 32, L15S01, https://doi.org/10.1029/2005GL022386, 2005.

Bognar, K., Zhao, X., Strong, K., Boone, C. D., Bourassa, A. E, Degenstein, D. A., Drummond, J. R., Duff, A., Goutail, F., Griffin, D., Jeffery, P. S., Lutsch, E., Manney, G., McElroy, C. T., Mclinden, C., Millán, L. F., Pazmino, A., Sioris, C., Walker, K. A., Zou, J.: Updated validation of ACE and OSIRIS ozone and NO2 measurements in the Arctic using ground-based instruments at Eureka, Canada. Journal of Quantitative Spectroscopy and Radiative Transfer. 238. https://doi.org/10.1016/j.jqsrt.2019.07.014, 2019.

Boone, C. D., Bernath, P. F., Lecours, M.: Version 5 retrievals for ACE-FTS and ACE-imagers, Journal of Quantitative Spectroscopy and Radiative Transfer,Volume 310, 108749, ISSN 0022-4073, https://doi.org/10.1016/j.jqsrt.2023.108749, 2023.

Burrows, J. P., Dehn, A., Deters, B., Himmelmann, S., Richter, A., Voigt, S., and Orphal, J.: Atmospheric remote-sensing reference data from GOME: Part 1. Temperature-dependent absorption cross-sections of NO2 in the 231–794 nm range, J. Quant. Spectrosc. Radiat. Transfer 60, 1025–1031, https://doi.org/10.1016/S0022-4073(97)00197-0, 1998.

Burrows, J. P., Richter, A., Dehn, A., Deters, B., Himmelmann, S., Voigt, S., and Orphal, J.: Atmospheric remote-sensing reference data from GOME—2. Temperature-dependent absorption cross sections of O3 in the 231–794 nm range, J. Quant. Spectrosc. Radiat. Transfer 61, 509–517, https://doi.org/10.1016/S0022-4073(98)00037-5, 1999.

Chance, K. and Kurucz, R. L.: An improved high-resolution solar reference spectrum for Earth's atmosphere measurements in the ultraviolet, visible, and near infrared, Journal of Quantitative Spectroscopy and Radiative Transfer, 111, 1289-1295, https://doi.org/10.1016/j.jqsrt.2010.01.036, 2010.

Dahl, H., Eliuk, W., Rumbold, G., Shelly, R.: ACE - A Canadian Small Satellite Mission, Proceedings of the 13th AIAA/USU Conference on Small Satellites, Aug. 23-26, Logan UT, SSC99-V-7, URL: http://digitalcommons.usu.edu/cgi/viewcontent.cgi?article=2151&context=smallsat, 1999.

Damadeo, R. P., Zawodny, J. M., Thomason, L. W., and Iyer, N.: SAGE version 7.0 algorithm: application to SAGE II, Atmos. Meas. Tech., 6, 3539–3561, https://doi.org/10.5194/amt-6-3539-2013, 2013.

https://doi.org/10.5194/egusphere-2025-4636
Preprint. Discussion started: 14 October 2025

Dupuy, E., Walker, K. A., Kar, J., Boone, C. D., McElroy, C. T., Bernath, P. F., Drummond, J. R., Skelton, R., McLeod, S. D., Hughes, R. C., Nowlan, C. R., Dufour, D. G., Zou, J., Nichitiu, F., Strong, K., Baron, P., Bevilacqua, R. M., Blumenstock, T., Bodeker, G. E., Borsdorff, T., Bourassa, A. E., Bovensmann, H., Boyd, I. S., Bracher, A., Brogniez, C., Burrows, J. P., Catoire, V., Ceccherini, S., Chabrillat, S., Christensen, T., Coffey, M. T., Cortesi, U., Davies, J., De Clercq, C., Degenstein, D. A., De Mazière, M., Demoulin, P., Dodion, J., Firanski, B., Fischer, H., Forbes, G., Froidevaux, L., Fussen, D., Gerard, P., Godin-Beekmann, S., Goutail, F., Granville, J., Griffith, D., Haley, C. S., Hannigan, J. W., Höpfner, M., Jin, J. J., Jones, A., Jones, N. B., Jucks, K., Kagawa, A., Kasai, Y., Kerzenmacher, T. E., Kleinböhl, A., Klekociuk, A. R., Kramer, I., Küllmann, H., Kuttippurath, J., Kyrölä, E., Lambert, J.-C., Livesey, N. J., Llewellyn, E. J., Lloyd, N. D., Mahieu, E., Manney, G. L., Marshall, B. T., McConnell, J. C., McCormick, M. P., McDermid, I. S., McHugh, M., McLinden, C. A., Mellqvist, J., Mizutani, K., Murayama, Y., Murtagh, D. P., Oelhaf, H., Parrish, A., Petelina, S. V., Piccolo, C., Pommereau, J.-P., Randall, C. E., Robert, C., Roth, C., Schneider, M., Senten, C., Steck, T., Strandberg, A., Strawbridge, K. B., Sussmann, R., Swart, D. P. J., Tarasick, D. W., Taylor, J. R., Tétard, C., Thomason, L. W., Thompson, A. M., Tully, M. B., Urban, J., Vanhellemont, F., Vigouroux, C., von Clarmann, T., von der Gathen, P., von Savigny, C., Waters, J. W., Witte, J. C., Wolff, M., and Zawodny, J. M.: Validation of ozone measurements from the Atmospheric Chemistry Experiment (ACE), Atmos. Chem. Phys., 9, 287-343, https://doi:10.5194/acp-9-287-2009, 2009.

EO Portal: SciSat-1 / ACE (Science Satellite/Atmospheric Chemistry Experiment), https://www.eoportal.org/satellite-missions/scisat-1#spacecraft, 2025, accessed on July 6, 2025.

Gilbert, K. L., Turnbull, D. N., Walker, K. A., Boone, C. D., McLeod, S. D., Butler, M., Skelton, R., Bernath, P. F., Chateauneuf, F., and Soucy, M.-A.: The onboard imagers for the Canadian ACE SCISAT-1 mission, J. Geophys. Res., 112, D12207, https://doi.org/10.1029/2006JD007714, 2007.

Jeffery, P. S., Drummond, J. R., McElroy, C. T., Walker, K. A., and Zou, J.: Validation of the version 4.5 MAESTRO ozone and NO2 measurements, Atmos. Meas. Tech., 18, 569–602, https://doi.org/10.5194/amt-18-569-2025, 2025.

Kar, J., McElroy, C. T., Drummond, J. R., Zou, J., Nichitiu, F., Walker, K. A., Randall, C. E., Nowlan, C. R., Dufour, D. G., Boone, C. D., Bernath, P. F., Trepte, C. R., Thomason, L. W., and McLinden, C.: Initial comparison of ozone and NO2 profiles from ACE-MAESTRO with balloon and satellite data, J. Geophys. Res.,112, D16301, https://doi.org/10.1029/2006JD008242, 2007.

Khanal, S., Toohey, M., Bourassa, A., McElroy, C. T., Sioris, C., and Walker, K. A.: Assessment of ACE-MAESTRO v3.13 multi-wavelength stratospheric aerosol extinction measurements, EGUsphere [preprint], https://doi.org/10.5194/egusphere-2024-3286, 2024.

Lucke, R. L., Korwan, D., Bevilacqua, R. M., Hornstein, J. S., Shettle, E. P., Chen, D. T., Daehler, M., Lumpe, J. D., Fromm, M. D., Debrestian, D., Neff, B., Squire, M.,König-Langlo, G., and Davies, J.: The Polar Ozone and Aerosol Measurement (POAM III) Instrument and Early Validation Results, J. Geophys. Res., 104, 18785–18799, https://doi.org/10.1029/1999JD900235, 1999.

McCormick, M. P., Zawodny, J. M., Veiga, R. E., Larsen, J. C., and Wang, P. H.: An overview of SAGE I and II ozone measurements, Planetary Space Sci., 37, 1567–1586, https://doi.org/10.1016/0032-0633(89)90146-3, 1989.

McCormick, M. P., Lei, L., Hill, M. T., Anderson, J., Querel, R., and Steinbrecht, W.: Atmos. Meas. Tech., 13, 1287–1297, 2020, https://doi.org/10.5194/amt-13-1287-2020.

McElroy, C. T., Nowlan, C., Drummond, J. R., Bernath, P. F., Barton, D., Dufour, D., Midwinter, C., Hall, R., Ogyu, A., Ullberg, A., Wardle, D., Kar, J., Zou, J., Nichitiu, F., Boone, C., Walker, K., and

https://doi.org/10.5194/egusphere-2025-4636
Preprint. Discussion started: 14 October 2025

Rowlands, N.: The ACE-MAESTRO instrument on SCISAT: description, performance, and preliminary results, Appl. Opt. 46, 4341-4356, https://doi.org/10.1364/AO.46.004341, 2007.

Nowlan, C. R., McElroy, C. T., Drummond, J. R.: Measurements of the O2 A- and B-bands for determining temperature and pressure profiles from ACE–MAESTRO: Forward model and retrieval algorithm, Journal of Quantitative Spectroscopy & Radiative Transfer, 108, 371–388, https://doi:10.1016/j.jqsrt.2007.06.006, 2007.

Russell, J. M., Gordley, L. L., Park, J. H., Drayson, S. R., Tuck, A. F., Harries, J. E., Cicerone, R. J., Crutzen, P. J., and Frederick, J. E.: The Halogen Occultation Experiment, J. Geophys. Res., 98, 10777–10797, https://doi.org/10.1029/93JD00799, 1993.

Sioris, C. E., Boone, C. D., Bernath, P. F., Zou, J., McElroy, C. T., and McLinden, C. A.: Atmospheric Chemistry Experiment (ACE) observations of aerosol in the upper troposphere and lower stratosphere from the Kasatochi volcanic eruption, J. Geophys. Res., 115, D00L14, https://doi:10.1029/2009JD013469, 2010.

Sioris, C. E., Zou, J., McElroy, C. T., McLinden, C. A., and Vömel, H.: High vertical resolution water vapour profiles in the upper troposphere and lower stratosphere retrieved from MAESTRO solar occultation spectra, Adv. Space Res., 46, 642–650, https://doi.org/10.1016/j.asr.2010.04.040, 2010.

Sioris, C. E., Zou, J., McElroy, C. T., Boone, C. D., Sheese, P. E., and Bernath, P. F.: Water vapour variability in the high-latitude upper troposphere – Part 2: Impact of volcanic eruptions, Atmos. Chem. Phys., 16, 2207–2219, https://doi:10.5194/acp-16-2207-2016, 2016.

Wang, H.-J., Cunnold, D. M., Trepte, C., Thomason, L. W., and Zawodny, J. M.: SAGE III solar ozone measurements: Initial results, Geophys. Res. Lett., 33, L03805, https://doi.org/10.1029/2005GL025099, 2006.

Walker, K. A., Zou, J., Nichitiu, F., Gilbert, K. L., Turnbull, D., McElroy, C. T., Evans, W. F. J., Ferguson, C., Puckrin E., Boone, C., McLeod, S. D., Butler, M., Midwinter, C., Drummond, J. R., and Bernath, P. F.: Science Commissioning of the Atmospheric Chemistry Experiment (ACE), Earth Observing Systems IX, edited by William L. Barnes, James J. Butler, Proc. SPIE 5542 (SPIE, Bellingham, WA, 2004), https://doi.org/10.1117/12.559941, 2004.

Robert, C. É., Bingen, C., Vanhellemont, F., Mateshvili, N., Dekemper, E., Tétard, C., Fussen, D., Bourassa, A., and Zehner, C.: AerGOM, an improved algorithm for stratospheric aerosol extinction retrieval from GOMOS observations – Part 2: Intercomparisons, Atmos. Meas. Tech., 9, 4701-4718, https://doi.org/10.5194/amt-9-4701-2016, 2016.